THE AMERICAN MINERALOGIST, VOL. 50, SEPTEMBER, 1965

STABILITY OF BIOTITE: EXPERIMENT, THEORY, AND APPLICATION[1]

DAVID R. WONES, *U. S. Geological Survey, Washington, D. C.*

AND

HANS P. EUGSTER, *Department of Geology, The Johns Hopkins University, Baltimore, Maryland.*

ABSTRACT

Biotites on the join phlogopite-annite react to form a number of assemblages and the reactions are governed by the independent intensive parameters, temperature, fugacity of H_2O (f_{H_2O}), and fugacity of oxygen (f_{O_2}). The most common of these assemblages in natural occurrences are biotite-sanidine-hematite; biotite-sanidine-magnetite; and biotite-leucite-olivine-magnetite. The compositions of biotites coexisting with sanidine and magnetite were determined for a variety of conditions of f_{H_2O}, f_{O_2} and temperature. The compositions lie in the ternary system $KFe_3^{2+}AlSi_3O_{10}(OH)_2$, annite-$KMg_3^{2+}AlSi_3O_{10}(OH)_2$, phlogopite-$KFe_3^{3+}AlSi_3O_{12}$ (H_{-1}), "oxybiotite."

Application of regular solution theory to $KFe_3AlSi_3O_{10}(OH)_2$ in ternary solid solution yields the following relationship:

$$\log f_{H_2O} = \frac{3428 - 4212\,(1 - x_1)^2}{T} + \log x_1 + 1/2 \log f_{O_2} + 8.23 - \log a_{KAlSi_3O_8} - \log a_{Fe_3O}$$

where x_1 is the mol fraction of $KFe_3AlSi_3O_{10}(OH)_2$ in biotite, $a_{KAlSi_3O_8}$ is the activity of $KAlSi_3O_8$ in the various mineral phases, and $a_{Fe_3O_4}$ is the activity of Fe_3O_4 in the various mineral phases. Neither molecular ($a = x$) or cationic ($a = x^3$) ideal solution theory describes the activities of $KFe_3AlSi_3O_{10}(OH)_2$ in "ternary" biotite solid solutions. The position of the f_{O_2}-T curves for biotite-muscovite-magnetite-corundum/alumino-silicate-quartz assemblages were determined by the intersections of the stability curves of biotite and muscovite. Schematic f_{O_2}-T curves are given for biotite-sanidine-pyroxene-magnetite-quartz assemblages.

Biotite crystallizing from a magma may follow either a more iron-rich trend or a more magnesium-rich trend, depending upon the f_{O_2} conditions during cooling. If f_{O_2} is decreasing with temperature, the Mg/Fe ratios of the anhydrous phases and the amount of magnetite either decrease or change very little. The magnesium-rich trend in the biotite compositions is represented by constant or increasing f_{O_2} (through loss of hydrogen) and leads to an increase in the amount of magnetite present and in the Mg-Fe ratios of the associated ferromagnesian phases. The two trends may represent, respectively, undersaturation or saturation of the melt in regard to H_2O.

Extrapolation to natural biotites assumes that Ti, Al, and F substitutions are similar to Mg, Fe^{+3}, and O substitutions. Biotite-K-feldspar-magnetite assemblages in low-grade metamorphic rocks (<500° C.) imply either disequilibrium or low H_2O pressures. Assemblages in the gneisses of the northwest Adirondacks imply H_2O fugacities of 0.1–10 bars and CO_2 fugacities of 400–10,000 bars during recrystallization of the interbedded gneisses and marbles.

Intersections of biotite f_{H_2O}-T curves with the "granite minimum melting curve" suggest that most biotite-bearing rhyolite and quartz latite magmas were at temperatures

[1] Publication authorized by the Director, U. S. Geological Survey.

greater than 750° C. and at H_2O pressures of less than 1000 bars just before extrusion. Biotite phenocrysts permit an estimate of minimum H_2O pressure in "granitic" melts; magnetite or orthopyroxene phenocrysts permit an estimate of maximum H_2O pressures.

Introduction

As biotites are very common constituents of igneous and metamorphic rocks, knowledge of biotite stabilities and phase equilibria should aid in the determination of certain boundary conditions (temperature, water pressure, oxygen pressure and compositional variations) for magmatic and metamorphic processes.

Previous investigators have determined the stability of the end members, phlogopite (Yoder and Eugster, 1954) and annite (Eugster and Wones, 1962), and this study attempts to examine the solid solution of those end members. The iron-magnesium ratio of biotites in igneous (Heinrich, 1946; Nockolds, 1947) and metamorphic (Thompson, 1957) rocks has been correlated with various rock types and grades of metamorphism, and this study establishes limitations of the intensive variables at which a particular biotite may be stable.

Cation substitution of Fe and Mg in silicate lattices has been discussed by Ramberg (1952), Mueller (1960), Bradley (1962), Bartholomé (1962), Ghose (1962) and Kretz (1964). Experimental studies have been limited to olivine and pyroxene equilibria, chiefly at liquidus temperatures and one atm. pressure (Bowen and Schairer, 1935; Muan and Osborne, 1955) whereas this study presents data on Mg-Fe substitutions in a hydrous silicate at elevated pressures. It may, therefore, serve as a model for other Mg-Fe solid solutions of hydrous silicates.

The present study is an attempt to define the biotite-sanidine-magnetite-gas equilibrium as a function of T, $P(\approx P_{H_2}+P_{H_2O})$, f_{O_2}, and phase composition at temperatures between 400° and 900° C. On biotite compositions, at f_{O_2} values between the Fe_3O_4-Fe_2O_3 and $Fe_{1-x}O$-Fe_3O_4 buffers, no other assemblages were encountered at the above conditions.

This manuscript presents the experiments, their interpretation, and methods of extrapolation in the first part. In the second part applications to some natural assemblages are discussed. The biotite assemblages will provide, if properly studied, definite limits on the possible temperatures and fugacity of components such as H_2O, O_2, and H_2 in geologic processes.

Experimental Techniques

The techniques used have been discussed by Eugster and Wones (1962) and Wones (1963b). Cold-seal hydrothermal apparatus supplied temperature and pressure. Pressure measurements were good to 1% and

the temperature control and measurement was within 5° C. of the stated temperature. Individual experiments were quenched by slow cooling (20 minutes) of a sealed pressure vessel. As reaction rates are very slow, this technique created no problems related to "quench phases."

Oxygen fugacities were controlled by the buffer technique of Eugster (1957). Table 1 lists the values of oxygen fugacity for the several buffers. Muan's (1963) results on the system Pd-Ag-Fe demonstrate the usefulness of Pd-Ag alloys in hydrothermal experiments with iron-bearing systems. $Pd_{30}Ag_{70}$ alloys were used only in the most recent experiments.

Phase equilibria were determined by examination of quenched products obtained from experiments using biotite or phlogopite+sanidine +magnetite as starting materials. The phlogopite, sanidine and magnetite were synthesized as pure phases and then mixed mechanically to avoid any ambiguity in results. The critical determination in all experiments is the composition of the biotite coexisting with sanidine, magnetite and gas.

TABLE 1. OXYGEN FUGACITIES OF OXYGEN BUFFERS (EUGSTER AND WONES, 1962)

Buffer	$\log f_{O_2} = -\frac{A}{T} + B + \frac{C(P-1)}{T}$		
	A	B	C
Fe_2O_3-Fe_3O_4	24912	14.41	0.019
Fe_3O_4-$Fe_{1-x}O$	32730	13.12	0.083
NiO-Ni	24709	8.94	0.046
SiO_2-Fe_2SiO_4-Fe_3O_4	27300	10.30	0.092

The exact location of the equilibrium is dependent upon attaining equilibrium by oxidizing a ferroan biotite to a magnesian biotite-sanidine-magnetite assemblage, and by reducing a phlogopite-sanidine-magnetite assemblage to a ferroan biotite-sanidine-magnetite assemblage. Complete reversibility was established for five points in addition to the data for the annite end member. The remainder of the data were obtained by oxidizing a biotite. Such experiments should yield a maximum iron content. All indications are that they approach equilibrium within 48–100 hours, whereas the reversing equilibrium requires at least 250 hours.

A sequence of experiments tabulated in Table 3c at 750° C. and 800° C., 2070 bars, demonstrates that the approach to equilibrium proceeded at highly variable rates. At 750° C., a 24-hour reducing experiment pro-

duced a biotite with $Fe/Fe+Mg=0.63$ whereas a 195-hour reducing experiment produced a biotite with a value of $Fe/Fe+Mg$ of 0.56. The value produced by oxidation of a ferroan biotite is 0.78 and is probably nearer the true equilibrium value. Where a large spread between oxidation and reduction experiments exists, the oxidation value is used.

Experiments using oxide mixes as starting materials were given little credence. They were only used in close conjunction with experiments using biotites or phlogopite-sanidine-magnetite as starting materials.

Composition of Phases

As methods of extrapolation and interpolation of the biotite phase equilibria depend heavily on assumptions concerning the purity of sanidine and magnetite, and on the composition of the gas phase, as well as the biotite composition, discussion of the compositional variations of all the phases is warranted.

Biotites. Biotite compositions were determined by measuring indices of refraction and the $(060,33\bar{1})$ x-ray spacing using the data of Wones (1963b). Optical measurements proved the most useful, as the x-ray reflections are weak and broadened by reflections from the inclusions of original biotite flakes within the newly crystallized sanidine. The method of Gower (1957) was not used as the (004) biotite reflection is coincident with the (311) of magnetite.

A complicating factor in this study has been the formation of "oxybiotite" in the biotite solid solutions. Consequently, the biotites are not a simple binary $KMg_3AlSi_3O_{10}(OH)_2$-$KFe_3AlSi_3O_{10}(OH)_2$ but rather they are members of the reciprocal system (Ricci, 1951, p. 371–389) $KMg_3AlSi_3O_{10}(OH)_2$-$3KFe^{2+}Fe_2^{3+}AlSi_3O_{12}$-$KFe_3^{2+}AlSi_3O_{10}(OH)_2$-$3KMg\cdot Fe_2^{3+}AlSi_3O_{12}$. If the theoretical (and physically impossible) composition, $KFe_3^{3+}AlSi_3O_{12}(H_{-1})$, is used as a component, then the biotite compositions can be plotted in the additive ternary system shown in Fig. 1. The shaded area represents those compositions that are physically impossible. The advantage of this type of plot is that the annite concentrations are assigned with simplicity, whereas in the reciprocal system they may be ambiguous in certain cases.

The concentrations of "oxybiotite" have not been rigorously determined. However, as Wones (1963b) demonstrated, the c axis of the unit cell contracts with increasing "oxybiotite" content. This has not been well calibrated, but the available data in the above study indicate that c contracts about 0.002 Å for each per cent "oxybiotite." Figure 1 plots the estimated position of the biotite solid solutions for each of the buffer

systems investigated. It should be emphasized that these curves represent little more than an "educated guess."

Another possible substitution is that of "ferriannite," $KFe_3^{2+}Fe^{3+}Si_3O_{10}(OH)_2$ (Wones, 1963a). The formation of this component requires the formation of an aluminous phase and a change in the physical properties of the biotites. No aluminous phases such as muscovite or corundum were observed by optical or x-ray techniques. The compositions of natural biotites coexisting with feldspars, pyroxenes, olivines, and

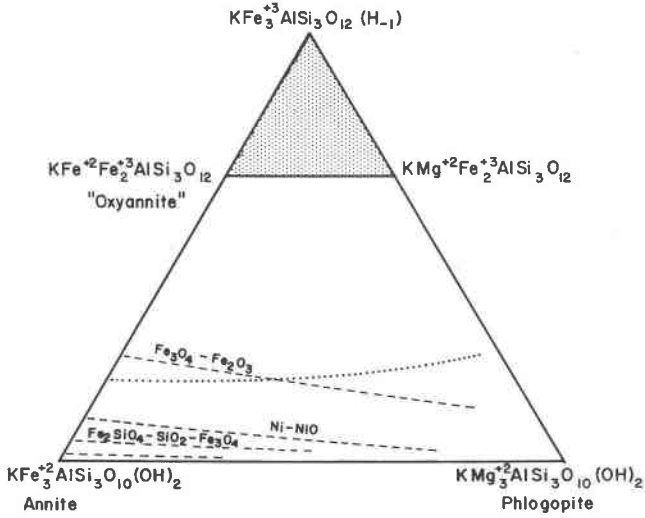

FIG. 1. The ternary system $KFe_3^{2+}AlSi_3O_{10}(OH)_2$-$KMg_3^{2+}AlSi_3O_{10}(OH)_2$-$KFe_3^{3+}AlSi_3O_{12}(H_{-1})$. Dashed lines indicated compositions of "buffered" biotites, the shaded area represents compositions physically impossible to obtain. Dotted line is that of appropriate composition of biotites that would provide a constant value for the heat of mixing.

magnetites (Heinrich, 1946; Nockolds, 1947) indicate that such a substitution is not to be expected.

In summary, the Fe/Fe+Mg ratio of the biotites has been determined with confidence, but the H_2 content is only estimated.

Feldspar. The expected variation in the feldspar compositions are either the $Fe^{3+} \rightleftharpoons Al^{3+}$ substitution resulting in $KFeSi_3O_8$ or solid solution of either Fe_3O_4 or Fe_2O_3 in $KAlSi_3O_8$. Measurements of the indices of refraction of feldspars (Table 2) are all within 0.002 of the ideal value for γ of 1.522 (Tuttle, 1952) and indicate less than 1 mol % $KFeSi_3O_8$ ($\gamma = 1.608$) (Wones and Appleman, 1961) and less than 0.4 mol % Fe_2O_3 ($\omega = 1.800$) (Deer *et al.*, 1962). The $KAlSi_3O_8$ polymorph is apparently high sanidine (Donnay and Donnay, 1952).

Magnetite. For the compositions studied, the possible types of substitutions causing deviations from the composition Fe_3O_4 are hercynite, $FeAl_2O_4$, maghemite, Fe_2O_3, and magnesioferrite, $MgFe_2O_4$. The first two, $FeAl_2O_4$ and Fe_2O_3, may be checked by unit cell measurements. The (333,511) reflection was measured for several magnetites at a variety of conditions, as well as for synthetic magnetites synthesized by the reduc-

TABLE 2. INDEX OF REFRACTION OF FELDSPARS AND $d_{\substack{333\\511}}$ OF MAGNETITIES COEXISTING WITH BIOTITES

T, ° C.	P, bars	Buffer	Starting Material[1]	Time, hrs.	γ, $KAlSi_3O_8$	$d_{\substack{333\\511}}$, Fe_3O_4
450	2070	Fe_3O_4-Fe_2O_3	annite	450	<1.523	n.d.
480	2070	Fe_3O_4-Fe_2O_3	ph+sa+mt	250	<1.5223	1.6159
550	1035	Fe_3O_4-Fe_2O_3	biotite	43	<1.524	n.d.
600	1035	Fe_3O_4-Fe_2O_3	biotite	42	<1.524	1.6161
620	2070	Fe_3O_4-Fe_2O_3	biotite	42	n.d.	1.6159
700	2070	Fe_3O_4-Fe_2O_3	Ox mix	65	<1.523	1.6160
800	2070	Fe_3O_4-Fe_2O_3	biotite	42	<1.523	n.d.
850	1035	Fe_3O_4-Fe_2O_3	biotite	28	<1.523	n.d.
700	1035	Ni-NiO	Fe mix	94	<1.525	n.d.
700	1035	Ni-NiO	biotite	105	n.d.	1.6158
750	2070	Ni-NiO	biotite	209	<1.523	n.d.
800	2070	Ni-NiO	Fe mix	121	<1.523	n.d.
800	2070	Ni-NiO	biotite	141	<1.524	n.d.
800	2070	Ni-NiO	ph+sa+mt	700	<1.523	1.6158
850	1035	Ni-NiO	Fe mix	92	<1.523	1.6159
725	2070	Fe_2SiO_4-SiO_2-Fe_3O_4	ph+sa+mt	168	<1.523	1.6159
750	1035	Fe_2SiO_4-SiO_2-Fe_3O_4	Fe mix	105	<1.523	1.6159
750	1035	Fe_2SiO_4-SiO_2-Fe_3O_4	biotite	142	<1.523	n.d.
750	1035	Fe_2SiO_4-SiO_2-Fe_3O_4	biotite	177	<1.523	1.6156
775	2070	Fe_2SiO_4-SiO_2-Fe_3O_4	ph+sa+mt	232	n.d.	1.6160
800	2070	Fe_2SiO_4-SiO_2-Fe_3O_4	biotite	250	<1.523	n.d.
800	2070	Fe_2SiO_4-SiO_2-Fe_3O_4	ph+sa+mt	250	<1.523	1.6159
850	1035	Fe_2SiO_4-SiO_2-Fe_3O_4	Fe mix	105	<1.523	1.6159
900	1035	Fe_2SiO_4-SiO_2-Fe_3O_4	biotite	6	<1.523	n.d.
850	1035	$Fe_{1-x}O$-Fe_3O_4	biotite	96	<1.523	1.6162

[1] Abbreviations: ph, phlogopite; sa, sanidine; mt, magnetite; Fe mix, $K_2O \cdot 6SiO_2$+Fe+MgO+Al_2O_3; Ox mix $K_2O \cdot 6SiO_2$+$FeC_2O_4 \cdot 2H_2O$+MgO+Al_2O_3.

tion of hematite or by oxidation and decomposition of $FeC_2O_4 \cdot 2H_2O$. The results are listed in Table 2. The value of $8.396 \pm .001$ Å for the unit cell edge of magnetite is larger than the value of 8.391 given by Turnock and Eugster (1962) or the value of 8.394 given by Robie and Bethke (1963). The important point is that none of the measurements deviate from the of value 8.396 by more than 0.0018. According to Turnock and Eugster this would indicate less than 0.5 mol per cent $FeAl_2O_4$ in solid solution. The Fe_2O_3 substitution only reaches measurable proportions at temperatures in excess of 900° C. The unit cell data indicate less than 1.8 mol per cent Fe_2O_3 (Donnay and Nowacki, 1954).

The $MgFe_2O_4$ content is a matter of great importance and cannot be resolved accurately by data on the unit cell (Deer *et al.*, 1962) although a limit of 10 mol per cent can be made. Three checks have been made on the $MgFe_2O_4$ content of the magnetites. First, all experiments in which $Fe/Fe+Mg=0.94$ yield large quantities of biotite. *If* the assemblage were only sanidine and magnetite, the maximum content of $MgFe_2O_4$ would be 18 mol per cent. In the second place, visual estimates of the biotite-magnetite ratio in such experiments indicate that the spinel is close to pure magnetite. Finally, in experiments within the hematite field of stability, no spinel phases were observed, indicating that $MgFe_2O_4$ is unstable in the presence of $KAlSi_3O_8$ and H_2O. However, in experiments buffered by magnetite-hematite assemblages, both iron oxides occurred in assemblages of biotite composition, indicating that the spinel phase would be pure Fe_3O_4. These several lines of evidence indicate that the spinel phase is essentially pure Fe_3O_4.

Gas. This phase is assumed to consist of the components H_2 and H_2O. Eugster and Wones (1962, p. 92–93) have considered the problems of estimating both the H_2 and H_2O contents, the fugacities of those components, and the amount of dissolved material in the gaseous phase. Eugster and Wones presented methods for computing f_{H_2O} and f_{H_2} at specified temperatures and pressures. Shaw and Wones (1964) have given new estimates of the fugacity coefficients of hydrogen, and these values have been used in this paper together with the fugacity coefficients for H_2O calculated by Holser (1954).

Shaw (1963a) has shown that H_2-H_2O mixtures are nonideal, but at the H_2/H_2O ratios encountered in this study, only the $Fe_{1-x}O$ buffered experiments have significant deviations from the ideal mixing assumed by Eugster and Wones (1962). As the hydrogen fugacity data are used extensively in determining activity coefficients and extrapolating the biotite data to lower temperatures, it is desirable to estimate the uncertainties in f_{H_2}. These are about 5% of the actual value, and are largely due to uncertainties in the data for the oxygen buffers, especially Fe_2SiO_4-Fe_3O_4-SiO_2.

Shaw's (1963a) results for the several oxygen buffers indicate that the Fe_2SiO_4-Fe_3O_4-SiO_2 data may be questionable and certainly need to be determined more rigorously. New data for Fe_3O_4-Fe_2O_3 have been published by Blumenthal and Whitmore (1961) using emf measurements of a magnetite-hematite cell. Their results yield oxygen fugacities 2 to 3 orders of magnitude greater than those given by Norton (1955). The magnetite prepared by Blumenthal and Whitmore, however, is probably

nonstoichiometric material enriched in Fe_2O_3, and hence, Norton's results are used.

In summary, the composition of sanidine is assumed to be $KAlSi_3O_8$, that of magnetite, Fe_3O_4, and the gas phase of variable ratios of H_2 and H_2O. There is no evidence for significant exchange of Fe and Al between sanidine and magnetite at the conditions of these experiments, and the amount of iron oxides dissolved in $KAlSi_3O_8$ must be less than 0.4 mol per cent.

Biotite compositions are expressed in two ways. The first is as $KFe_{3x}Mg_{3(1-x)}AlSi_3O_{10+y}(OH)_{2-y}$ where y (and therefore Fe^{2+}/Fe^{3+}) is undefined and x is the ratio Fe/Fe+Mg. The second method is $KFe_{3x_1}{}^{2+}Fe_{3x_3}{}^{3+}Mg_{3x_2}{}^{2+}AlSi_3O_{12}H(2\text{-}3x_3)$ where x_1 is the concentration of $KFe_3^{2+}AlSi_3O_{10}(OH)_2$, annite; x_2, $KMg_3AlSi_3O_{10}(OH)_2$, phlogopite; and x_3, $KFe_3^{3+}AlSi_3O_{12}(H_{-1})$, "oxybiotite." Throughout the remainder of this paper these definitions of x, x_1, x_2, and x_3 will be retained.

Experimental Results

The results of individual experiments are listed in Table 3 and the data for 1035 and 2070 bars total pressure are plotted in Figs. 2 and 3. The plots represent pseudobinary T-X projections for experiments buffered by several different assemblages and correspond to the lower portion of Fig. 14. It must be remembered that the oxygen and hydrogen contents change in these diagrams, but the elements remain in the ratio K:Al:Si:(Fe, Mg) of 1:1:3:3.

The value of the experiments varies as a function of starting material, length of time of the experiment, and precision of the compositional determinations. The location of the determined equilibrium points is tabulated in Table 4 with the hydrogen fugacity of the experiment and the estimated "oxybiotite" contents.

An important feature of the data is that the reversed equilibria, although few in number, do provide sufficient constraints on the unreversed approaches to equilibrium to permit judicious use of the latter data. Hence the boundary curves given in Figs. 2 and 3 represent a combination of reversed equilibria, nonreversed experiments approaching equilibrium, and interpretation.

A plot of these data in an f_{O_2}-T projection is given in Fig. 4. Contours represent the compositions of biotites which coexist with sanidine and magnetite for a given value of T and f_{O_2}. The contour labelled 100 bounds the field of stability of annite from Eugster and Wones (1962) and the contour O represents the upper stability limit of phlogopite and was calculated from the data of Yoder and Eugster (1954). Luth (1964) pre-

TABLE 3. EXPERIMENTS DETERMINING COMPOSITION (Fe/Fe+Mg) OF BIOTITES COEXISTING WITH SANIDINE AND MAGNETITE

T(° C.)	P (bars)	Time (hrs.)	Starting Material (Fe/Fe+Mg)	Final Biotite Composition				Remarks
				α	γ	d_{060}	Fe/Fe+Mg	
a) Experiments buffered by the assemblage Fe_3O_4—Fe_2O_3								
875	1035	8	bio(0.352)	1.591	1.646	1.5396	0.32± .06	
850	1035	28	bio(0.352)	1.587	1.634	1.5396	0.30± .04	
800	1035	66	bio(0.169)	1.571	1.602	1.5379	0.17± .02	no reaction
800	1035	45	bio(0.352)	1.587	1.634	1.5391	0.30± .05	
800	1035	42	bio(0.550)	1.582	1.628	1.5392	0.30± .05	
800	1035	48	bio(0.765)	1.582	1.628	n.d.	0.30± .05	
800	1035	50	bio(0.765)	1.582	1.628	1.5418	0.30± .05	
775	1035	61	bio(0.352)	n.d.	1.629	n.d.	0.35± .05	no reaction
750	1035	70	bio(0.352)	1.586	1.627	1.5397	0.35± .02	no reaction
750	1035	38	bio(0.550)	n.d.	1.628	1.5397	0.36± .05	
750	1035	42	bio(0.765)	n.d.	1.622	1.5397	0.34± .05	
700	1035	64	bio(0.169)	1.566	1.600	1.5380	0.17± .02	no reaction
700	1035	44	bio(0.550)	n.d.	1.630	n.d.	0.38± .04	
700	1035	250	ph+sa+mt(0.765)	n.d.	1.631	n.d.	0.38± .02	reversed reaction
675	1035	69	bio(0.550)	n.d.	1.631	n.d.	0.39± .02	
650	1035	94	bio(0.550)	n.d.	(1.612)	n.d.	0.39± .05	agg. index of refraction
650	1035	94	bio(0.765)	n.d.	(1.607)	n.d.	0.35± .07	agg. index of refraction
650	1035	70	bio(0.765)	n.d.	(1.614)	n.d.	0.41± 05	agg. index of refraction
620	1035	44	bio(0.765)		1.667		0.66± .03	
600	1035	63	bio(0.169)	1.561	1.600	1.5384	0.17± .02	no reaction
600	1035	139	bio(0.352)	1.582	1.621	1.5411	0.35± .02	no reaction
600	1035	94	bio(0.550)	1.591	1.645	1.5426	0.55± .02	some hematite
600	1035	42	bio(0.765)		1.654		0.56± .04	
550	1035	140	bio(0.550)	1.586	1.646	1.5432	0.55± .02	no reaction
550	1035	43	bio(0.765)		1.665		0.65± .04	only hematite
500	1035	64	bio(0.550)	1.576	1.641	1.5455	0.55± .02	no reaction
500	1035	83	bio(0.765)	1.621	1.673	1.5486	0.77± .02	no reaction
485	1035	42	bio(0.765)	1.625	1.679	1.5484	0.77± .02	no reaction
900	2070	6.5	bio(0.352)	n.d.	1.633	1.5388	0.27± .05	

TABLE 3—(*continued*)

T(° C.)	P (bars)	Time (hrs.)	Starting Material (Fe/Fe+Mg)	Final Biotite Composition				Remarks
				α	γ	d_{060}	Fe/Fe+Mg	
800	2070	71	bio(0.169)	n.d.	1.613	1.5373	0.17± .02	no reaction
800	2070	73	bio(0.352)	1.581	1.634	1.5391	0.35± .02	no oxides
800	2070	28	bio(0.550)	1.584	1.630	1.5390	0.35± .04	
800	2070	43	bio(0.550)	1.580	1.630	1.5397	0.35± .04	
800	2070	42	bio(0.765)	1.587	1.632	n.d.	0.37± .04	
750	2070	51	bio(0.550)		1.632		0.37± .04	
750	2070	42	bio(0.765)		1.635	1.5417	0.41± .03	
725	2070	67	bio(0.550)		1.626		0.33± .03	Only hematite
700	2070	47	bio(0.169)	1.571	1.605	1.5375	0.17± .02	no reaction
700	2070	122	bio(0.352)	1.581	1.628	1.5399	0.35± .02	no reaction
700	2070	68	bio(0.550)		1.634		0.39± .03	
700	2070	122	bio(0.550)		1.629		0.36± .03	
700	2070	40	Ox mix(0.765)		1.627		0.35± .03	
700	2070	65	bio(0.765)		1.637		0.43± .03	
680	2070	64	Ox mix(0.765)		1.633		0.40± .04	
680	2070	42	bio(0.765)		1.640		0.44± .04	
650	2070	94	bio(0.550)	1.596	1.651	1.5430	0.55± .02	some hematite present
650	2070	113	bio(0.765)		1.639		0.45± .04	
625	2070	94	bio(0.765)		1.640		0.46± .04	
600	2070	115	bio(0.169)	1.569	1.591	1.5374	0.17± .02	no reaction
600	2070	73	bio(0.352)	1.576	1.623	1.5397	0.35± .02	no reaction
600	2070	94	bio(0.550)	1.591	1.645	1.5426	0.55± .02	some hematite and magnetite present
600	2070	89	bio(0.765)		1.649		0.52± .02	
570	2070	65	bio(0.765)		1.667		0.66± .03	
550	2070	45	bio(0.765)		1.674		0.72± .03	only hematite
520	2070	72	bio(0.765)		1.680		0.77± .02	no reaction
500	2070	159	bio(0.880)		(1.657)		0.80± .05	(Agg. index of refraction
			b) Experiments buffered by the assemblage Ni—NiO					
850	1035	816	ph+sa+mt(0.765)		1.672		0.40± .04	reversed reaction
850	1035	138	bio(0.352)	1.582	1.622		0.35± .02	no reaction
850	1035	94	bio(0.765)		1.637		0.46± .04	
850	1035	92	Fe mix(0.880)		1.631		0.43± .05	

TABLE 3—(*continued*)

T(° C.)	P (bars)	Time (hrs.)	Starting Material (Fe/Fe+Mg)	Final Biotite Composition				Remarks
				α	γ	d_{060}	Fe/Fe+Mg	
800	1035	210	Fe mix(0.550)	1.589	1.629	1.5466	0.44± .03	
800	1035	165	bio(0.550)	1.589	1.636	1.5436	0.47± .05	
800	1035	123	Fe mix(0.765)	1.593	1.636	1.5494	0.49± .05	
750	1035	116	bio(0.880)		1.643		0.54± .03	
700	1035	320	bio(0.550)		1.647	1.5487	0.55± .02	no reaction
700	1035	94	bio(0.765)		1.622	1.5493	0.69± .02	
700	1035	105	bio(0.880)		1.654		0.63± .03	
700	1035	116	Fe mix(0.880)		1.660		0.68± .02	
800	2070	118	bio(0.169)	1.564	1.597	1.5387	0.17± .02	no reaction
800	2070	121	bio(0.352)	1.575	1.612	1.5440	0.35± .02	no reaction
800	2070	168	bio(0.550)	1.599	1.643	1.5479	0.55± .02	no reaction
800	2070	700	ph+sa+mt(0.765)	1.595	1.651	1.5468	0.56± .04	reversed reaction
800	2070	140	bio(0.765)	1.596	1.642	1.5471	0.54± .04	
800	2070	178	bio(0.880)	1.597	1.642	1.5469	0.55± .03	
800	2070	118	bio(0.880)	1.598	1.646	1.5496	0.56± .06	
800	2070	160	bio(0.939)		1.642		0.53± .03	
750	2070	209	bio(0.765)		1.663		0.70± .03	
750	2070	597	ph+sa+mt(0.765)		1.650		0.60± .03	reversed reaction
750	2070	209	bio(0.880)		1.660		0.67± .03	
750	2070	209	bio(0.939)		1.658		0.66± .03	
700	2070	139	bio(0.169)	1.564	1.597	1.5385	0.17± .02	no reaction
700	2070	139	bio(0.352)	1.575	1.616	1.5410	0.35± .02	no reaction
700	2070	179	bio(0.550)	1.595	1.654	1.5475	0.55± .02	no reaction
700	2070	160	bio(0.765)	1.620	1.673	1.5518	0.77± .02	no reaction
700	2070	1110	ph+sa+mt(0.765)		1.642		0.53	reversed reaction
700	2070	132	bio(0.880)		1.683		0.88± .04	magnetite present
700	2070	164	Fe mix(0.880)		1.676		0.82± .03	
650	2070	336	ph+sa+mt(0.765)		1.673		0.77± .02	complete reversal
650	2070	89	bio(0.765)		1.673	1.5511	0.77± .02	no reaction
600	2070	92	bio(0.765)	1.623	1.668	1.5519	0.77± .02	no reaction
600	2070	132	bio(0.880)	1.622	1.681	1.5534	0.88± .02	no reaction
600	2070	140	bio(0.939)	1.628	1.690	1.5549	0.94± .02	no reaction
			c) Experiments buffered by the assemblage Fe_2SiO_4—Fe_3O_4—SiO_2					
900	1035	6	bio(0.550)	1.591	1.646	1.5450	0.50± .05	
850	1035	94	bio(0.352)	1.581	1.622	1.5445	0.35± .02	no reaction
850	1035	129	bio(0.550)	1.595	1.644		0.54± .04	
850	1035	105	Fe mix(0.550)	1.592	1.636		0.49± .02	
850	1035	105	Fe mix(0.765)	1.587	1.629		0.42± .04	
800	1035	250	ph+sa+mt(0.765)	1.586	1.632		0.43± .02	reversed reaction

TABLE 3—(*continued*)

T(°C.)	P (bars)	Time (hrs.)	Starting Material (Fe/Fe+Mg)	Final Biotite Composition				Remarks
				α	γ	d_{060}	Fe/Fe+Mg	
800	1035	94	bio(0.550)		1.644		0.55± .02	no reaction
800	1035	49	bio(0.765)		1.644		0.54± .04	
800	1035	89	Fe mix(0.880)	1.602	1.650		0.61± .03	
800	1035	123	Fe mix(0.880)	1.596	1.637		0.52± .04	
775	1035	229	ph+sa+mt(0.765)		1.635		0.46± .04	reversed reaction
750	1035	229	ph+sa+mt(0.765)		1.642		0.52± .04	reversed reaction
750	1035	91	bio(0.550)		1.644		0.55± .02	no reaction
750	1035	86	bio(0.765)		1.660		0.67± .04	
750	1035	176	bio(0.880)		(1.644)		0.75± .05	(agg. index ref)
700	1035	250	ph+sa+mt(0.765)		1.665		0.71± .04	reversed reaction
700	1035	229	ph+sa+mt(0.765)		1.672		0.77± .02	complete reaction
850	2070	132	bio(0.352)	1.570	1.612		0.25± .04	no oxides present
825	2070	118	bio(0.352)	1.580	1.620	1.5442	0.35± .02	no reaction
800	2070	89	bio(0.352)	1.578	1.617	1.5432	0.35± .02	no reaction
800	2070	122	bio(0.550)	1.600	1.648	n.d.	0.55± .02	no reaction
800	2070	432	ph+sa+mt	1.607	1.664		0.70± .02	reversed reaction
800	2070	250	ph+sa+mt	1.591	1.639		0.49± .02	reversed reaction
800	2070	142	bio(0.765)	1.607	1.664		0.70± .02	
800	2070	65	bio(0.765)	1.603	1.666		0.69± .04	
800	2070	48	bio(0.880)	1.605	1.660		0.67± .04	
775	2070	96	bio(0.765)		1.672		0.77± .02	no reaction
775	2070	24	ph+sa+mt(0.765)		1.645		0.54± .04	reversed reaction
750	2070	89	bio(0.550)	1.597	1.643	1.5489	0.55± .02	no reaction
750	2070	231	ph+sa+mt(0.765)		1.655		0.63± .04	reversed reaction
750	2070	195	ph+sa+mt(0.765)		1.647		0.56± .04	reversed reaction
750	2070	122	ph+sa+mt(0.765)		1.650		0.59± .04	reversed reaction
750	2070	71	bio(0.765)		1.672		0.77± .02	no reaction
750	2070	48	ph+sa+mt(0.765)		1.654		0.62± .04	reversed reaction
750	2070	24	ph+sa+mt(0.765)		1.655		0.63± .04	reversed reaction
750	2070	48	bio(0.880)		1.673		0.78± .02	
740	2070	74	bio(0.765)		1.672		0.77± .02	no reaction

TABLE 3—(*continued*)

T(°C.)	P (bars)	Time (hrs.)	Starting Material (Fe/Fe+Mg)	Final Biotite Composition				Remarks
				α	γ	d_{060}	Fe/Fe+Mg	
725	2070	168	ph+sa+mt(0.765)		1.655		0.63± .04	reversed reaction
725	2070	167	bio(0.765)		1.677	1.5509	0.77± .02	no reaction
715	2070	92	bio(0.880)	1.623	1.684	1.5546	0.88± .02	no reaction
700	2070	92	bio(0.352)	1.575	1.616	1.5435	0.35± .02	no reaction
700	2070	150	bio(0.550)	1.597	1.644	1.5478	0.55± .02	no reaction
700	2070	450	bio(0.765)	1.612	1.670	1.5514	0.77± .02	no reaction
700	2070	250	ph+sa+mt(0.765)		1.655		0.63± .04	reversed reaction
700	2070	113	bio(0.880)	1.620	1.682	1.5544	0.88± .02	no reaction
700	2070	140	bio(0.939)	1.629	1.690	1.550	0.94± .02	no reaction
			d) Experiments buffered by the assemblage $Fe_{1-x}O$—Fe_3O_4					
850	1035	177	bio(0.550)	1.597	1.646	1.5475	0.55± .02	no reaction
850	1035	94	bio(0.765)	1.615	1.666	1.5516	0.72± .04	
850	1035	96	bio(0.765)	1.615	1.666	1.5507	0.72± .04	

sents a revision of these data. The phlogopite contour curves sharply at low f_{O_2} values, because the gas phase becomes increasingly enriched in hydrogen and the fugacity (and activity) of H_2O decreases rapidly. Hydrogen acts as an inert gas with respect to the phlogopite decomposition, but because f_{H_2O} decreases with decreasing f_{O_2}, the decomposition temperature must be lowered. This points up the important fact that equilibria of hydrous silicates free of iron are also subject to the composition of the gas phase and therefore to changes in f_{O_2}, if an appreciable amount of hydrogen is present.

The high temperature relationships are further complicated by the fact that silicate melts form at those conditions (Luth, 1964). The sanidine+magnetite+biotite assemblages will react, with increasing temperatures to form leucite+olivine+magnetite+biotite assemblages, kalsilite+leucite+olivine assemblages, or olivine+melt assemblages.

The contours of biotite compositions have been interpolated from Fig. 3 and Table 3. Only those portions of the contours which are well established by the experimental data are shown. The shapes of complete contours are suggested in Fig. 13. Because of the temperature limitations, contours are complete within the magnetite field only for iron-rich biotites ($Fe/Fe+Mg \times 100 \geq 70$), but they do extend to magnesium-rich biotites in the upper portion of the magnetite field. A particular contour indicates that a biotite of that Fe/Fe+Mg ratio is stable anywhere below that contour, but not above it, where the biotite is replaced by the assemblage magnesian biotite-sanidine-magnetite.

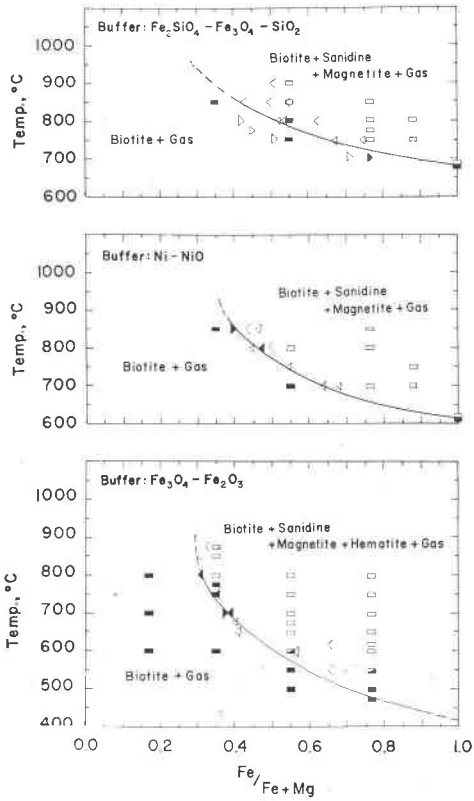

FIG. 2. Position of biotite-sanidine-magnetite-gas equilibria at 1035 bars total pressure as a function of temperature and Fe/Fe+Mg at oxygen fugacities of the given buffer assemblages. Open blocks represent biotite-sanidine-magnetite assemblages; shaded blocks, biotite assemblages; partially shaded blocks, biotite-sanidine-hematite assemblages. Brackets and triangles indicate composition of biotites coexisting with sanidine and magnetite. Shaded triangles represent high reliability, open triangles fair reliability, open brackets low reliability.

Consider a biotite with (Fe/Fe+Mg×100) of 70. This biotite (and all biotites for which Fe/Fe+Mg×100≤70) is stable at any value of f_{O_2} and T on or below the 70 contour. If an increase in f_{O_2} (or decrease in T) above (below) this contour occurs, the originally homogeneous biotite must react under O_2 to form magnetite, sanidine, and H_2O and a biotite whose composition is given by the contour appropriate to the new f_{O_2}-T conditions. The amount of magnetite and sanidine formed during oxidation can be calculated from the initial and final composition of the biotite. Thus, the decomposition of biotite to biotite-sanidine-magnetite at 2070 bars is defined between 400° and 900° C. by Fig. 4. A similar figure can be con-

structed for 1035 bars from Fig. 2. For a given biotite composition, the assemblage biotite-sanidine-magnetite-gas is divariant in the system $KAlSi_3O_8$-MgO-Fe-O-H and is represented by a curved surface in the f_{O_2}-f_{H_2O}-T space. A more complete f_{O_2}-T diagram will be discussed later (Fig. 13). The most important feature of Fig. 4 is the steep intersections

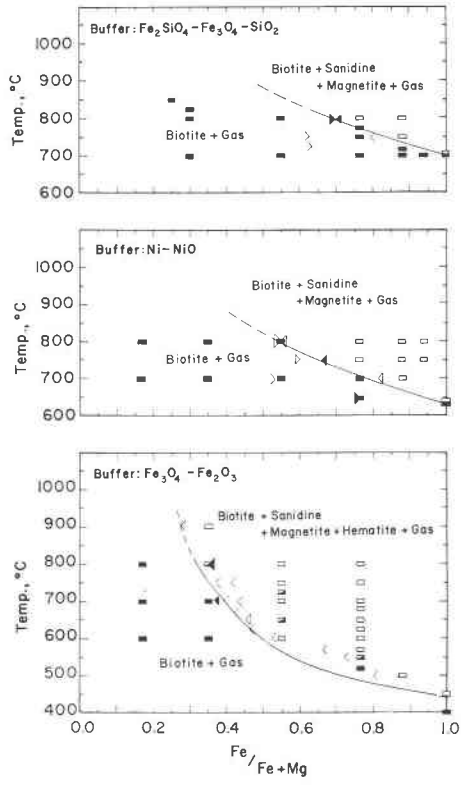

FIG. 3. Position of biotite-sanidine-magnetite-gas equilibria at 2070 bars total pressure. Symbols are the same as in Fig. 2.

of the biotite curves with the "buffer" curves. Presumably the stability curves of most of the anhydrous ferromagnesian silicates will be parallel to the "buffer" curves, so that the resulting assemblages of biotites and other ferromagnesian minerals for a given bulk composition are highly dependent on f_{O_2}, f_{H_2O} and temperature.

In effect, the biotites represent a two-volatile equilibrium, the two volatiles being oxygen and water. Consequently the effect of temperature changes on biotite compositions is very dependent on the activities of the

TABLE 4. POSITION OF THE DIVARIANT ASSEMBLAGE BIOTITE-SANIDINE-MAGNETITE-GAS AS DETERMINED IN THIS STUDY

Log $a_{KFe_3AlSi_3O_{10}(OH)_2}$	T, ° C.	P, bars	Buffer	log f_{H_2}	Fe	Estimated values[1]			Remarks
					Fe+Mg	x_1	x_2	x_3	
−4.563	900	2070	Fe_3O_4-Fe_2O_3	−1.477	0.27	0.14	0.73	0.13	single experiment
−4.530	850	1035	Fe_3O_4-Fe_2O_3	−1.799	0.30	0.16	0.70	0.14	single experiment
−4.186	787	1035	Fe_3O_4-Fe_2O_3	−1.842	0.32	0.17	0.68	0.14	average of 775° and 800° C.
−3.922	800	2070	Fe_3O_4-Fe_2O_3	−1.578	0.35	0.20	0.65	0.15	
−3.814	750	1035	Fe_3O_4-Fe_2O_3	−1.896	0.35	0.20	0.65	0.15	
−3.564	750	2070	Fe_3O_4-Fe_2O_3	−1.646	0.37	0.22	0.63	0.15	
−3.398	700	1035	Fe_3O_4-Fe_2O_3	−1.949	0.38	0.23	0.62	0.15	reversed equilibrium
−3.160	700	2070	Fe_3O_4-Fe_2O_3	−1.711	0.39	0.24	0.61	0.15	
−3.153	675	1035	Fe_3O_4-Fe_2O_3	−1.964	0.39	0.24	0.61	0.15	
−2.919	650	1035	Fe_3O_4-Fe_2O_3	−1.990	0.40	0.25	0.60	0.15	large uncertainty in composition
−2.692	650	2070	Fe_3O_4-Fe_2O_3	−1.763	0.45	0.29	0.55	0.16	single experiment
−2.391	600	1035	Fe_3O_4-Fe_2O_3	−2.042	0.56	0.38	0.44	0.18	
−2.181	600	2070	Fe_3O_4-Fe_2O_3	−1.832	0.54	0.37	0.46	0.17	
−1.900	850	1035	Ni-NiO	0.831	0.41	0.37	0.59	0.04	reversed equilibrium
−1.799	550	1035	Fe_3O_4-Fe_2O_3	−2.100	0.65	0.46	0.35	0.19	single experiment
−1.561	800	1035	Ni-NiO	0.783	0.47	0.42	0.53	0.05	
−1.450	850	1035	Fe_2SiO_4-SiO_2-Fe_3O_4	1.281	0.49	0.47	0.51	0.02	
−1.307	800	2070	Ni-NiO	1.037	0.56	0.50	0.44	0.06	reversed equilibrium
−1.189	750	1035	Ni-NiO	0.729	0.54	0.49	0.46	0.05	single experiment
−1.053	800	1035	Fe_2SiO_4-SiO_2-Fe_3O_4	1.291	0.55	0.52	0.45	0.03	
−1.006	500	2070	Fe_3O_4-Fe_2O_3	−2.091	0.80	0.61	0.20	0.19	
−0.954	750	2070	Ni-NiO	0.964	0.66	0.59	0.34	0.07	reversed equilibrium
−0.825	800	2070	Fe_2SiO_4-SiO_2-Fe_3O_4	1.519	0.70	0.66	0.30	0.04	reversed equilibrium
−0.778	700	1035	Ni-NiO	0.671	0.69	0.62	0.31	0.07	
−0.633	750	1035	Fe_2SiO_4-SiO_2-Fe_3O_4	1.285	0.70	0.66	0.30	0.04	
−0.555	700	2070	Ni-NiO	0.894	0.82	0.74	0.18	0.08	
−0.488	850	1035	$Fe_{1-x}O$-Fe_3O_4	2.243	0.72	0.70	0.28	0.02	
−0.417	750	2070	Fe_2SiO_4-SiO_2-Fe_3O_4	1.501	0.78	0.74	0.22	0.04	

[1] x_1 = mol fraction $KFe_3^{2+}AlSi_3O_{10}(OH)_2$; x_2, $KMg_3AlSi_3O_{10}(OH)_2$; x_3, $KFe_3^{3+}AlSi_3O_{12}(H_{-1})$.

two volatile constituents. However, the activities of oxygen and water are related to that of hydrogen by the dissociation of water, and useful results are obtained in considering the hydrogen-biotite equilibrium.

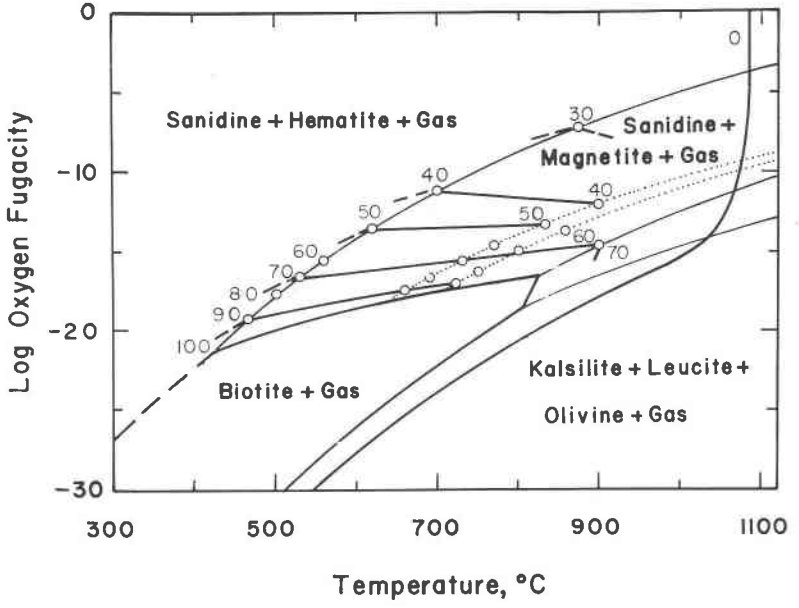

FIG. 4. A projection from the Fe/Fe+Mg axis of the biotite equilibria onto the f_{O_2}-T plane at 2070 bars total pressure. The positions of biotite-sanidine-magnetite equilibria as determined in this study are shown by heavy contours of constant Fe/Fe+Mg×100 values for the biotites and are taken from Fig. 3. Heavy curve labeled O represents maximum phlogopite stability, area bounded by curve labeled 100 is the annite stability field. Light weight lines and dotted lines represent "buffer" curves (see Table 1). See also Figs. 13 and 14.

BIOTITE SOLID SOLUTIONS; ACTIVITY COEFFICIENTS

The reaction between annite and sanidine and magnetite can be written as follows:

$$\underset{\text{annite}}{KFe_3AlSi_3O_{10}(OH)_2} \rightleftharpoons \underset{\text{sanidine}}{KAlSi_3O_8} + \underset{\text{magnetite}}{Fe_3O_4} + \underset{\text{gas}}{H_2} \qquad \text{(I)}$$

Eugster and Wones (1962) derived an expression relating hydrogen fugacity to temperature for that reaction. Using the hydrogen fugacity coefficients of Shaw and Wones (1964), that expression becomes

$$\log f^{\circ}_{H_2} = -\frac{9341}{T} + 11.05\ (\pm 0.11) \qquad (1)$$

where T is in °K.

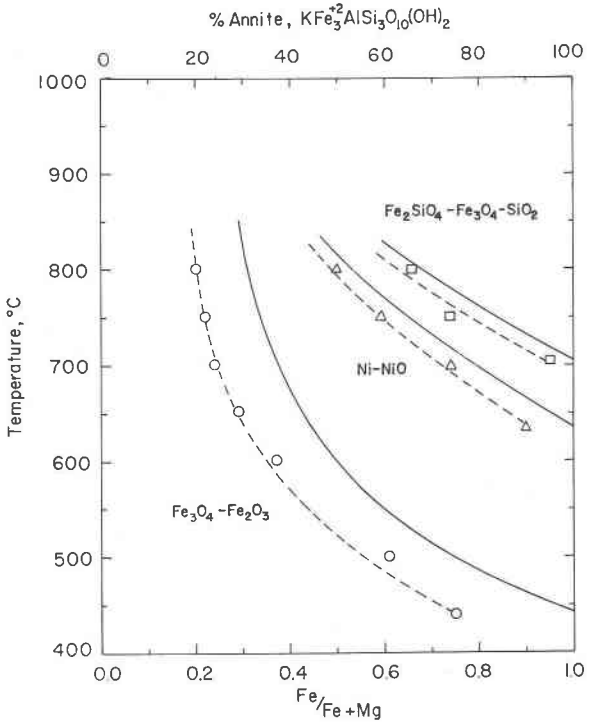

FIG. 5. Comparison of annite concentration (mol per cent)-temperature data and Fe/Fe+Mg-temperature data for biotites coexisting with sanidine, magnetite, and gas (H_2+H_2O) at a total pressure of 2070 bars. Solid lines indicate Fe/Fe+Mg data; dashed lines, annite concentration data. Solid lines are from Fig. 3, dashed curves are based on the data of Table 4. Circles indicate points buffered by Fe_3O_4-Fe_2O_3; triangles, Ni-NiO; squares, Fe_2SiO_4-Fe_3O_4-SiO_2.

As all of the phases present are pure end members (assuming for the present that "oxyannite" is of low concentration), equation (1) is equally well an expression for an equilibrium constant, K_{annite}, where

$$\log K_{annite} = \log \frac{a_{KAlSi_3O_8} \cdot a_{Fe_3O_4} \cdot f_{H_2}}{a_{KFe_3AlSi_3O_{10}(OH)_2}} = -\frac{9341}{T} + 11.05\ (\pm 0.11) \qquad (1')$$

We may now use equation (1′) to define the standard state for $KFe_3AlSi_3O_{10}(OH)_2$ keeping in mind the problem of variations in the quantity of "oxyannite" in the solid solution.

The effects of total pressure are very small. From the compilation of Robie and Bethke (1963), the molar volumes (cc/mol) are Fe_3O_4, 44.53; $KAlSi_3O_8$, 108.98; and $KFe_3AlSi_3O_{10}(OH)_2$, 154.32. This results in a volume change of about 1 cc/mole for the solids, which corresponds to

~25 calories/1000 bars. Wones (1963b) has demonstrated the partial molar volume of $KFe_3AlSi_3O_{10}(OH)_2$ in biotite solid solutions to be a constant, so that all $P\Delta V_{solid}$ terms may be neglected.

As can be seen from the data in Table 4 the $KFe_3AlSi_3O_{10}(OH)_2$ concentration of the biotites coexisting with sanidine and magnetite are not directly equivalent to the Fe/Fe+Mg (or x) ratios because of the presence of "oxybiotite" (x_3). This difference is shown very clearly in Fig. 5 where $KFe_3AlSi_3O_{10}(OH)_2$ concentration (x_1)-temperature plots are compared with the Fe/Fe+Mg-temperature plots for 2070 bars. When no "oxybiotite" is present, $x = x_1$. The deviations are not serious for Ni-NiO and Fe_2SiO_4-Fe_3O_4-SiO_2 buffered assemblages, but they are quite large for the Fe_3O_4-Fe_2O_3 data. For this reason, the $KFe_3AlSi_3O_{10}(OH)_2$ concentration rather than Fe/Fe+Mg will be used henceforth in the derivation of activity coefficients. Figure 5 again points up the fact that, at a given temperature, biotites from biotite-sanidine-magnetite assemblages are much more iron-rich at low values of f_{O_2} and that this effect is more pronounced at lower temperatures.

The activity of $KFe_3AlSi_3O_{10}(OH)_2$, $a_{KFe_3AlSi_3O_{10}(OH)_2}$, in a solid solution of biotite coexisting with sanidine, magnetite and gas, may be readily obtained through expression (1′):

$$a_{KFe_3AlSi_3O_{10}(OH)_2} = \frac{f_{H_2}}{f^{\circ}_{H_2}} \tag{2}$$

where f_{H_2} is the fugacity of hydrogen in the particular biotite assemblage and $f^{\circ}_{H_2}$ is the fugacity of H_2 in the analogous assemblage containing pure annite at the same temperature. Values of log $a_{KFe_3AlSi_3O_{10}(OH)_2}$ are given in Table 4.

Plots of log $a_{KFe_3AlSi_3O_{10}(OH)_2}$ versus log x and log x_1 are given in Fig. 6 and 7. If the biotites are ideal molecular solutions of $KFe_3AlSi_3O_{10}(OH)_2$, $KMg_3AlSi_3O_{10}(OH)_2$, and $KFe_3^{3+}AlSi_3O_{10}(H_{-1})$, then the activities would be characterized by $a = x$ or $a = x_1$. However, an ideal cationic substitution (Bradley, 1962), in the three octahedral sites would correspond to $a = x^3$ or $a = x_1^3$. As can be seen from Figs. 6 and 7 neither solution is adequate. Figure 7 also demonstrates that the variable x_1 gives a consistency to all data, whereas in Fig. 6 the variable x leads to a discontinuity between data collected with the different buffers. This consistency suggests a model of random mixing of 3 moles of (Fe, Mg) over two distinct sites, but until further work is done, another model is proposed for extrapolation. Consequently x_1 is the appropriate variable, as it is the concentration of $KFe_3AlSi_3O_{10}(OH)_2$, the component whose standard state is defined by equation (1′).

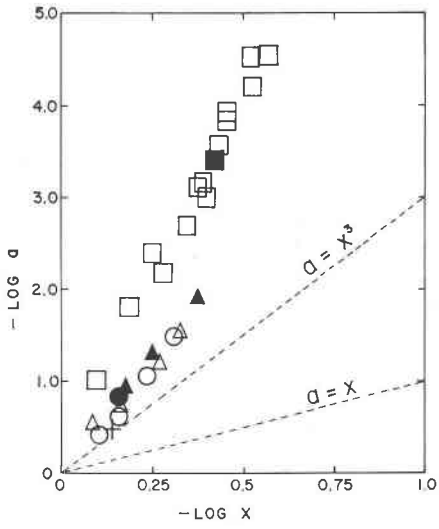

FIG. 6. Logarithm of the activity of $KFe_3AlSi_3O_{10}(OH)_2$ plotted as a function of the logarithm of Fe/Fe+Mg of biotites (X) coexisting with sanidine and magnetite. Squares represent experiments buffered by Fe_3O_4-Fe_2O_3; triangles, Ni-NiO; circles, Fe_2SiO_4-Fe_3O_4-SiO_2; crosses, $Fe_{1-x}O$-Fe_3O_4. Solid symbols represent reversed equilibria. The lower line ($a=x$) represents molecular ideal solution theory; the upper line ($a=x^3$), ideal cationic substitution theory.

The activity coefficient for $KFe_3AlSi_3O_{10}(OH)_2$, γ_1, is derived from the following relationship:

$$a = \gamma_1 x_1 = \frac{f_{H_2}}{f^\circ_{H_2}}; \qquad \log \gamma_1 = \log f_{H_2} - \log f^\circ_{H_2} - \log x_1 \tag{3}$$

If cationic substitutions are used:

$$3 \log \gamma_1 = \log f_{H_2} - \log f^\circ_{H_2} - 3 \log x_1 \tag{3'}$$

As the number of substitutions is not merely the octahedral cation substitutions, but also involve the $O \rightleftharpoons OH$ anionic substitution, a molecular model has been used to describe the activity of $KFe_3AlSi_3O_{10}(OH)_2$ in the solid solutions considered here.

The theory of regular solutions (Guggenheim, 1952) was applied to the data with some success, but the problem of the "oxybiotite" content has prevented final resolution of the problem until better data on the concentration of that component are obtained. From regular solution theory

$$\log \gamma_1 = \frac{(1 - x_1)^2 W}{2.303\ RT} \tag{4}$$

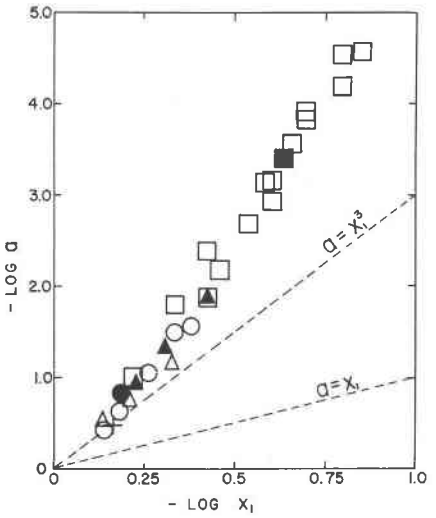

FIG. 7. Logarithm of the activity of $KFe_3AlSi_3O_{10}(OH)_2$ plotted as a function of the logarithm of the mol fraction of $KFe_3AlSi_3O_{10}(OH)_2(x_1)$. Symbols are identical to Figure 6.

where W is the heat of mixing per mole. Figure 8 is a plot of log γ_1 versus $(1-x_1)^2/T$. The slope is about -4212, and from this a heat of mixing of -870 cal/mole has been derived. The lack of agreement between the high temperature Fe_3O_4-Fe_2O_3 buffered data and the remainder of the data may be due to any one or all of the following:

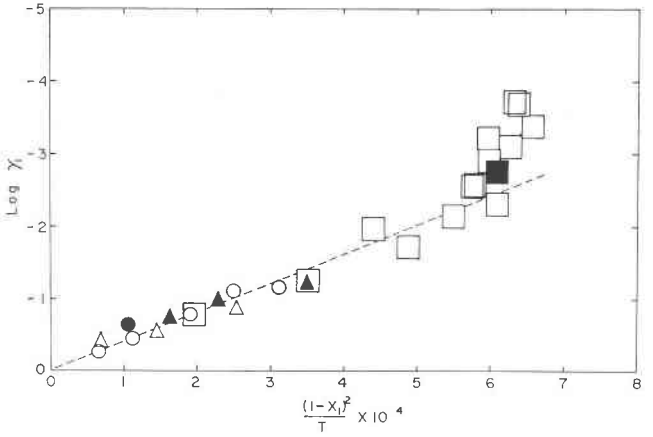

FIG. 8. Logarithm of the activity coefficient of $KFe_3AlSi_3O_{10}(OH)_2(a/x_1)$ plotted as a function of $(1-x_1)^2/T$. Symbols are identical to Fig. 6.)

(1) because of their short duration, the high temperature experiments do not represent equilibrium; (2) the fundamental values for the f_{O_2} of the Fe_3O_4-Fe_2O_3 equilibria given by Norton (1955) are incorrect; (3) the heat of mixing of the oxybiotite-annite substitutions is a function of composition; or (4) the estimates of the "oxybiotite" compositions are incorrect, due either to inefficient calibration of the physical properties or to changes during the quench procedures. If (4) were the main problem, the appropriate composition of the biotites in the ternary system which would provide a constant value for the heat of mixing are plotted as a dotted line in Fig. 1. In our opinion both (3) and (4) could be responsible for the observed discrepancies in Fig. 8.

Until more precise work is done on the composition, regular solution theory provides a satisfactory empirical model for the energy of mixing of $KFe_3AlSi_3O_{10}(OH)_2$ "molecules" in a biotite solid solution series where the $KFe_3AlSi_3O_{10}(OH)_2$ concentration is greater than 25 mole percent (Fig. 8; Table 4). The activity of $KFe_3AlSi_3O_{10}(OH)_2$ in a solid solution series is given by combining equations (3) and (4):

$$\log a_{KFe_3AlSi_3O_{10}(OH)_2} = \log x_1 - \frac{4212\,(1-x_1)^2}{T}\ (\pm 0.20) \tag{5}$$

For biotites coexisting with sanidine and magnetite, an expression for the hydrogen fugacity may be obtained by combining equation (1′) and (5):

$$\log f_{H_2} = -\frac{9341 + 4212\,(1-x_1)^2}{T} + \log x_1 + 11.05\ (\pm 0.20) \tag{6}$$

Adding an approximation for the equilibrium constant for H_2O, the following expression is obtained:

$$\log f_{H_2O} = \frac{3428 - 4212\,(1-x_1)^2}{T} + \log x_1 + 1/2 \log f_{O_2} + 8.23\ (\pm 0.20) \tag{6′}$$

For an assemblage containing impure K-feldspar and impure magnetite the expression expands to:

$$\log f_{H_2O} = \frac{3428 - 4212\,(1-x_1)^2}{T} + \log x_1 + 1/2 \log f_{O_2} + 8.23 - \log a_{KAlSi_3O_8} - \log a_{Fe_3O_4}\ (\pm 0.20) \tag{6″}$$

The agreement between regular solution theory and the actual run data is shown in Fig. 9, a plot of hydrogen fugacity versus the inverse temperature (° K). The actual run data (Table 4) are given as well as the curves calculated from equation (6) for the several mol fractions of $KFe_3AlSi_3O_{10}(OH)_2$. Biotite is stable on the right hand side of the curves and biotite-sanidine-magnetite-hydrogen on the left hand side. Individual points give the mol fraction of $KFe_3AlSi_3O_{10}(OH)_2$, taken from Table 4. The agreement with the curves calculated from regular solution theory seems very satisfactory.

A more direct comparison with respect to Fe/Fe+Mg ratios is given in Fig. 10 which is a comparison between the experimental curves,

regular solution theory curves, and molecular ideal curves at a total pressure of 2070 bars. The molecular proportions (mol % $KFe_2AlSi_3O_{10}(OH)_2$) were adjusted to Fe/Fe+Mg by means of Fig. 1. The data for

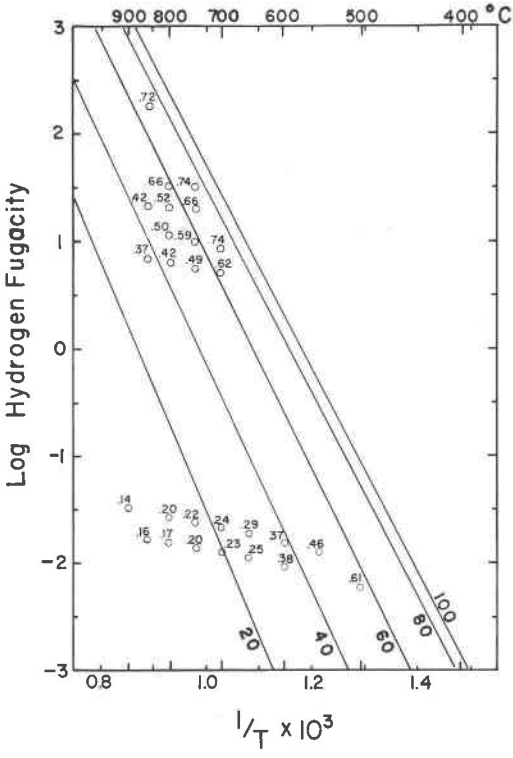

FIG. 9. Logarithm of hydrogen fugacity plotted as a function of inverse temperature (°K) and composition of biotite for biotite-sanidine-magnetite-gas assemblages. Open circles give the position of experimental points with determined biotite compositions. The lower group of points were determined at 1035 and 2070 bars with a Fe_3O_4-Fe_2O_3 buffer while the middle groups refer to Fe_2SiO_4-Fe_3O_4-SiO_2 and Ni-NiO data. (mol per cent $KFe_3AlSi_3O_{10}(OH)_2$). Heavy lines are equilibrium positions calculated by regular solution theory for specified values of mol per cent $KFe_3AlSi_3O_{10}(OH)_2$.

the Fe_3O_4-Fe_2O_3 assemblages show the deviation between predicted values and actual measured values. It is obvious that there is a close correspondence between measured values and regular solution values, except for biotites on the hematite-magnetite buffer above 600° C. It is equally obvious that an ideal solution model is far from satisfactory in describing biotite solid solutions.

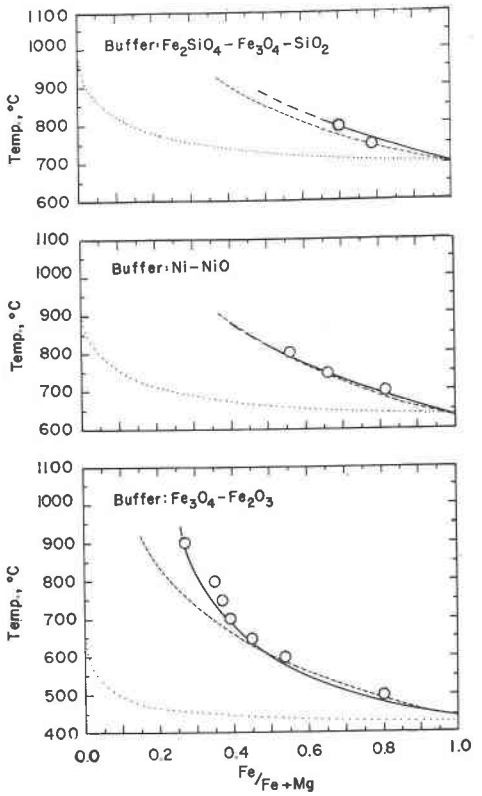

FIG. 10. Biotite composition-temperature plots comparing experimental results (circles and heavy lines), regular solution theory (dashed lines), and molecular ideal solution theory (dotted lines) for a total pressure of 2070 bars. Solid lines are from Fig. 3; circles from Table 4.

EXTRAPOLATION TO OTHER ASSEMBLAGES CONTAINING BIOTITE

Biotite-muscovite-magnetite-corundum or (Al_2SiO_5*-quartz*)*-gas.* Chinner's (1960) discussion of the gneisses and schists at Glen Clova, Scotland, pointed out that the interrelation of biotite-muscovite pairs need not be restricted to the considerations of chlorite and garnet reactions. The relation pertaining to oxygen fugacity as the intensive variable is the following:

$$KFe_3AlSi_3O_{10}(OH)_2 + Al_2O_3 + \tfrac{1}{2}O_2 = KAl_2AlSi_3O_{10}(OH)_2 + Fe_3O_4 \qquad \text{(II)}$$

annite corundum muscovite magnetite

or by adding quartz:

$$\underset{\text{annite}}{KFe_3AlSi_3O_{10}(OH)_2} + \underset{\text{sillimanite}}{Al_2SiO_5} + \tfrac{1}{2}O_2 = \underset{\text{muscovite}}{KAl_2AlSi_3O_{10}(OH)_2} + \underset{\text{magnetite}}{Fe_3O_4} + \underset{\text{quartz}}{SiO_2} \qquad \text{(III)}$$

the position of reaction (II) plotted as a function of f_{O_2} and T is given in Fig. 11. The position of the calculated points is obtained from the intersection of equation (6′) with the new data for the reaction $KAl_2AlSi_3O_{10}$

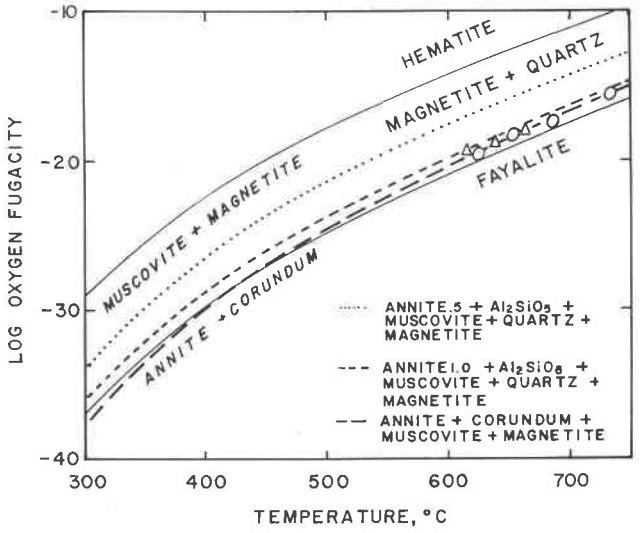

FIG. 11. Biotite+corundum$\rightleftharpoons$magnetite+muscovite and biotite+$Al_2SiO_5$$\rightleftharpoons$magnetite +muscovite+quartz oxidation reactions plotted as functions of f_{O_2} and temperature. Ellipses indicate intersections of the annite data of Eugster and Wones (1962) with that of Velde (1964) for muscovite. Triangles indicate intersection of annite data with that of Segnit and Kennedy (1962) for muscovite+quartz. Solid lines indicate boundaries between iron oxide and fayalite assemblages. The three dashed curves are calculated from equations (4), (8) and (9).

$(OH)_2$ (muscovite)$\rightleftharpoons KAlSi_3O_8$ (sanidine)$+Al_2O_3$ (corundum)$+H_2O$ (gas) obtained by Velde (1964). The temperature value obtained for a given f_{H_2O} by Velde was substituted with the value for f_{H_2O} in equation (6′) in order to obtain the f_{O_2} value at which annite (biotite), muscovite, sanidine, corundum and magnetite coexist at the given temperature (see ellipses in Figure 11).

Reaction (III) is also plotted in Fig. 11. The values of those plotted points were obtained by using the data of Segnit and Kennedy (1962) for the muscovite+quartz$\rightleftharpoons$K-feldspar+corundum+H_2O with equation (6′). The essential features of these reactions are that they are inde-

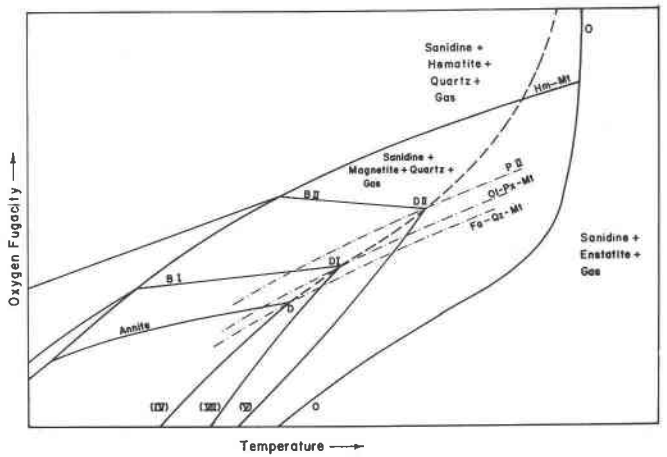

FIG. 12. Schematic f_{O_2}-T relationships for the bulk compositions biotite+3 quartz at some arbitrary value of total pressure ($P_{H_2}+P_{H_2O}$). Curves labeled "annite," BI, and BII represent biotites of arbitrary $KFe_3AlSi_3O_{10}(OH)_2$ content coexisting with sanidine, magnetite/hematite, and quartz. Curve labeled O is the boundary marked by the reaction phlogopite+3 quartz$\rightleftharpoons$sanidine+enstatite. Dash-dot curves represent the assemblages fayalite-quartz-magnetite (Fa-Qz-Mt), olivine-pyroxene-magnetite, (Ol-Px-Mt), and pyroxene-magnetite-quartz (PII). The dashed curve through points D, DI, and DII represents the maximum thermal stability of a given biotite in the presence of quartz. See discussion under "*Biotite-quartz-gas.*"

pendent of the activity of H_2O, are parallel to the other silicate f_{O_2}-T curves, and indicate that, in an aluminous environment, pure annite is stable with quartz and magnetite only over extremely limited f_{O_2}-T regions.

Approximate equations have been derived graphically for reactions (II):

$$\log f_{O_2} = -\frac{33000}{T(^\circ K.)} + 17.2 \pm 15\% \tag{8}$$

and (III):

$$\log f_{O_2} = -\frac{27000}{T(^\circ K.)} + 10.9 \pm 15\% \tag{9}$$

The effect of pressure is small as the ΔV_{solids} is about 5 cc/mol for reaction (II) and 3 cc/mol for reaction (III).

The effect of diluting the $KFe_3AlSi_3O_{10}(OH)_2$ component in biotite solid solutions is to displace the curves to higher values of f_{O_2} at constant temperature. The approximate curve representing the assemblage biotite (50 mole % $KFe_3AlSi_3O_{10}(OH)_2$)-muscovite-magnetite-Al_2SiO_5-quartz is plotted as the dotted line in Fig. 11. The maximum thermal

stability of both biotite and muscovite is a function of f_{H_2O}, and Fig. 11 was constructed with the assumption that f_{H_2O} was high enough for the micas to be stable.

Chinner (1960) has shown how the increased "oxygen content" in a biotite-quartz-muscovite-kyanite-magnetite-(hematite) gneiss corresponds to increases in f_{O_2}. In Fig. 11, for a given isotherm, the biotite

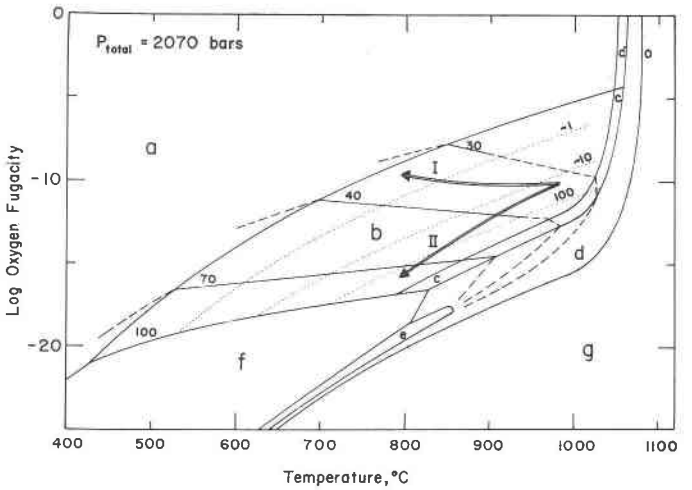

FIG. 13. Stability of biotites as a function of f_{O_2} and temperature compared to the approximate stability of olivines (and pyroxenes) at a total pressure (H_2+H_2O) of 2070 bars. The fields are labeled as follows: a) biotite-sanidine-hematite-(gas); b) biotite-sanidine-magnetite; c) biotite-leucite-olivine-magnetite (c′ = hematite); d) biotite-kalsilite-leucite-olivine; e) biotite-leucite-olivine-iron; f) biotite (annite); g) kalsilite-leucite-olivine. Solid and dashed lines show the stability of a given biotite (Fe/Fe+Mg×100); dotted lines, olivines. Biotite equilibria for a number of biotite bulk compositions have been projected along the Fe/Fe+Mg axis upon the f_{O_2}-T plane. Lables of fields are not unique and high temperature areas are labeled for magnesium-rich bulk compositions only. Arrows labeled I and II show oxidizing and reducing trends in crystalizing magmas.

composition will become more magnesium rich with increasing fugacity of oxygen, a relation recognized qualitatively by Chinner.

Tilley (1957), in a discussion of the alkalic rocks of the Haliburton-Bancroft area in Ontario, Canada, gives an analysis of a very iron-rich biotite. As this biotite coexists with corundum, the annite-corundum curve of Fig. 11 helps to define the intensive variables during crystallization of those rocks.

The curves representing these assemblages indicate that biotites with intermediate Fe/Fe+Mg ratios will be stable in a smaller range of f_{O_2}

and temperature values if they coexist with kyanite, sillimanite, andalusite, or corundum than if they exist in a non-aluminous environment. The f_{O_2}-T curve above which biotites with more than 50% annite cannot coexist with aluminous silicates lies somewhat above the curve for the Ni-NiO buffer. Figure 4 shows the contrasting curve for biotite (50% annite)-sanidine-magnetite assemblages.

Biotite-quartz-gas. The most common biotite-bearing mineral assemblages are those containing quartz. The stability of annite-quartz was determined by Eugster and Wones (1962) and we were able to show that it does not differ from the annite stability at f_{O_2} values above those of the Fe_2SiO_4-Fe_3O_4-SiO_2 buffer because the addition of quartz does not lead to the formation of new phases. The high-oxygen fugacity assemblages are hematite+sanidine+quartz and magnetite+sanidine+quartz. However, at f_{O_2} values below those of the Fe_2SiO_4-Fe_3O_4-SiO_2 buffer, the stability field of annite+quartz is drastically reduced, because of the reaction of quartz with magnetite to form fayalite. The annite+sanidine +magnetite+quartz boundary terminates at the intersection with that buffer curve, represented by point D in Fig. 12 (for the magnitudes of f_{O_2} and T of point D for a given P_{gas} see Eugster and Wones, 1962).

Below point D the annite+quartz field is bounded by the curve representing the reaction

$$\underset{\text{annite}}{KFe_3AlSi_3O_{10}(OH)_2} + 3/2\ \underset{\text{quartz}}{SiO_2} \rightleftharpoons \underset{\text{sanidine}}{KAlSi_3O_8} + 3/2\ \underset{\text{fayalite}}{Fe_2SiO_4} + H_2O \qquad \text{(IV)}$$

which originates at point D.

For bulk compositions of increasing magnesium content, fayalite is replaced at first by an iron-rich olivine and later by a pyroxene (see, for instance, Bowen and Schairer, 1935). Hence for biotites with intermediate Mg/Mg+Fe ratios, the biotite+quartz field must be bounded by a reaction of the type

$$\underset{\text{biotite BII}}{K(Fe, Mg)_3AlSi_3O_{10}(OH)_2} + 3SiO_2 \rightleftharpoons \underset{\text{sanidine}}{KAlSi_3O_8} + 3\underset{\text{pyroxene}}{(Fe, Mg)SiO_3} + H_2O \qquad \text{(V)}$$

The field boundary represented by this reaction must intersect the biotite+quartz+sanidine+magnetite boundary for the same biotite composition (B II) at a point D II (see Fig. 12). D II is also a point on the f_{O_2}-T curve representing the coexistence of the intermediate pyroxene of reaction V with magnetite and quartz (curve P II in Fig. 12). Any pyroxene richer in $FeSiO_3$ would be oxidized along this curve according to the reaction

$$\underset{\text{ferrosilite}}{3FeSiO_3} + 1/2\ O_2 \rightleftharpoons \underset{\text{magnetite}}{Fe_3O_4} + \underset{\text{quartz}}{3SiO_2} \qquad \text{(VI)}$$

No data are available on the oxidation of intermediate pyroxenes, but it is reasonable to assume, that the f_{O_2}-T curves for pyroxene-magnetite (or hematite)-quartz assemblages behave similar to those for the oxidation of intermediate olivines, which will be discussed later and are shown in Fig. 13. If they do behave in that way, they will lie essentially parallel to the oxygen buffer curves. They will also have the property that for iron-rich pyroxenes a large change in Fe/Fe+Mg will cause a small change in f_{O_2}, while for magnesium rich pyroxenes just the opposite is true.

Point D II of Fig. 12 represents the assemblage biotite+quartz +sanidine+pyroxene+magnetite. It is an isobaric invariant point and lies on the biotite+quartz contour B II, which is identical with the biotite contour of Fig. 4 for the same biotite composition. The composition of the pyroxene of point D II and curve P II is not known and will have to be established experimentally. The location of the biotite +quartz+sanidine+magnetite boundary is not known (reaction V), but it must originate in point D II and move subparallel to boundary IV towards lower values of f_{O_2} and T. Point D II, therefore, is the highest temperature, for a given P_{gas}, at which a biotite of composition B II can coexist with quartz.

Somewhere between points D and D II of Fig. 12, olivines must be replaced by pyroxenes. Point D I has been drawn to represent the assemblage biotite+olivine+pyroxene+sanidine+magnetite +quartz+gas. The following field boundaries, for a fixed bulk composition, biotite B I+quartz, intersect in point D I; biotite+quartz+sanidine+magnetite (B I), biotite+quartz+sanidine+olivine+pyroxene (VII) and olivine+pyroxene+magnetite+quartz (Ol-Px-Mt), whereby curve Ol-Px-Mt must lie between the f_{O_2}-T curve for the Fe_2SiO_4-Fe_3O_4-SiO_2 buffer and curve P II; but the difference in f_{O_2} between these two curves is probably exceedingly small (see discussion of Fig. 13).

Figure 12 also contains a contour labelled 0 which represents the assemblage phlogopite+quartz+enstatite+sanidine+gas. This contour behaves similarly to the phlogopite+forsterite+leucite+kalsilite+gas curve of Fig. 4, but lies at lower temperature for a given gas pressure. With increasing Mg content, the biotite+quartz contours of Fig. 12 (biotite+quartz+hematite+sanidine, biotite+quartz+magnetite +sanidine, and biotite+quartz+pyroxene+sanidine) must move towards higher temperatures without crossing each other and they will eventually, in the absence of iron, merge with the phlogopite+quartz contour (0). Therefore, the path described by all points D II must curve upwards and asymptotically approach the 0 contour at high f_{O_2} values.

Figure 12 has been drawn with the assumption that, at that particular gas pressure, enstatite+sanidine+gas is the stable high-temperature

assemblage. Recent data by Wones (unpublished) indicate that at a temperature of about 840° C. and a gas pressure of 2000 bars the assemblage phlogopite+quartz+enstatite+melt+gas is stable. Hence, of the biotite contours drawn for $P_{gas}=2000$ bars in Fig. 4, only those which lie at temperatures lower and at f_{O_2} values higher than the corresponding pyroxene-magnetite-quartz boundary (P II) remain unaffected by the addition of quartz. A similar argument holds for the reaction sanidine+quartz+gas$\rightleftharpoons$melt at temperatures above 765° C. (Shaw, 1963c).

Application to Natural Biotites

Determination of annite concentration. In the foregoing discussion of biotite reactions, emphasis has been on the end member annite, $KFe_3AlSi_3O_{10}(OH)_2$. In all assemblages concerning potassium-rich feldspar and/or muscovite and magnetite a critical variable is the $KFe_3AlSi_3O_{10}(OH)_2$ concentration. In most natural biotites, and especially those occurring in igneous rocks, the determination of the concentration of this component is a problem of some interest.

In examining analyses of natural biotites, one is immediately struck by the diversities in composition. There are three groups of cationic substitutions possible in biotites: "interlayer" substitutions ($K^+\rightleftharpoons Na^+\rightleftharpoons Ca^{2+}\rightleftharpoons H_3O^+$), octahedral layer substitutions ($Fe^{2+}\rightleftharpoons Mg^{2+}\rightleftharpoons Mn^{2+}\rightleftharpoons Fe^{3+}\rightleftharpoons Al^{3+}\rightleftharpoons Ti^{4+}\rightleftharpoons\square$ [vacancy]), and tetrahedral layer substitutions ($Si^{+4}\rightleftharpoons Al^{3+}\rightleftharpoons Fe^{3+}$). In addition there are the anionic substitutions ($OH^-\rightleftharpoons F^-\rightleftharpoons Cl^-\rightleftharpoons O^{2-}$). The problem remains of determining the concentration of $KFe_3AlSi_3O_{10}(OH)_2$ within a given biotite. For the ideal end member, the only inter-layer cation is K, the only octahedral cation is Fe^{2+}, Al occupies $\frac{1}{4}$ of the tetrahedral sites, and the anions are 2(OH) groups in addition to 10 oxygens. Decrease of any of the ideal quantities will decrease the concentration of $KFe_3AlSi_3O_{10}(OH)_2$ and affect the activity of that component.

A great deal of work will be required to establish the effect of other substitutions, but probably the (Na, Ca)$\rightleftharpoons$K and the $3Fe^{2+}\rightleftharpoons 2Al^{3+}+\square$ substitutions are the only ones which will tend to decrease the stability of annite. This deduction is based on the effect of paragonite component on the stability of muscovite (Eugster and Yoder, 1956) and the known limitation of solid solution between trioctahedral and dioctahedral micas (Foster, 1960).

Until more complete data on the effect of these substitutions are available, simplicity requires the determination of the maximum concentration of K, Fe^{2+}, [$AlSi_3$], and OH within their respective sites, and the assignment of the smallest of those concentrations to $KFe_3AlSi_3O_{10}(OH)_2$.

A cursory examination of most biotite analyses indicates that Fe^{2+} in the octahedral site is the most common limitation.

As the present study has been concerned with that substitution, it would seem that the determination of the mol fraction of Fe^{2+} in the octahedral layer and the substitution of that value for "x_1" in equations (5, 6) above is the most direct means of applying the results of this study to natural biotite assemblages.

A final remark may be in order concerning the use of physical properties to estimate the mol fraction of $KFe_3AlSi_3O_{10}(OH)_2$. The most easily measured properties are the unit cell dimensions, *x*-ray reflection intensities, the indices of refraction, density, and more recently, magnetic susceptibility.

The optical measurements are limited in that the birefringence of biotites changes very little, and in a majority of cases, 2V is so small as to provide very little information. This reduces the optical data to effectively one measurement and one or two estimates.

As pointed out by Smith and Yoder (1956), the majority of biotite unit cells have a β of $99°55' \pm 20'$ (1M) or $95°00'$ (2M) and $a\sqrt{3} \approx b$. Hence *b* and *c* provide two measurements.

The remaining properties (*x*-ray reflection intensities, density and magnetic susceptibility) may provide sufficient accurate data if done under optimum conditions with a great deal of care.

Hence 6 parameters are available to estimate some dozen common substitutions. Although there are some limiting effects, a chemical analysis still seems to be the most satisfactory technique and, with the present day advances in fluorescence spectrometry, will probably prove the simplest.

Recognition of useful mineral assemblages. The composition of a biotite within a given rock merely permits an estimation of either the maximum f_{O_2} or temperature or the minimum f_{H_2O} or f_{H_2} at which the biotite formed. This does not provide much more than an estimate of one or two variables, if the third is known or estimated.

However, the presence of the equilibrium assemblage sanidine-magnetite-biotite immediately permits the determination of the univariant f_{H_2}-T (or the divariant f_{O_2}-f_{H_2O}-T) conditions of the formation of the mineral assemblage which contains biotite of a specific composition. The analogous assemblage muscovite-corundum (aluminosilicate-quartz)-magnetite permits the determination of f_{O_2}-T conditions. Hence the critical determination of the presence of sanidine or muscovite, magnetite, quartz, and the aluminosilicates is most important in making full use of the biotite equilibrium data.

Perhaps one of the most useful applications of the biotite data is in establishing maximum (or minimum) H_2O activities in processes involving igneous (and some metamorphic) rocks. Here the divariant equilibrium involving f_{O_2}-f_{H_2O}-T (equation 6′) for the biotite-sanidine-magnetite assemblage is the one of interest. The presence of ilmenite with the magnetite permits an estimate of f_{O_2}-T conditions and the substitution of these in equations (6′) or (6″) then permits limits to be placed on f_{H_2O} (Lindsley, 1963).

In metamorphic assemblages the biotite+muscovite+magnetite+aluminosilicate+quartz assemblage permits f_{O_2}-T estimates independently of f_{H_2O}, (reactions II and III) and consequently does not permit the estimate of H_2O activities. However, if combined with chlorite:

$$KFe_3AlSi_3O_{10}(OH)_2 + Fe_5Al_2Si_3O_{10}(OH)_8 + 4/3\ O_2 \rightleftharpoons 3SiO_2 + KAl_2AlSi_3O_{10}(OH)_2 + 8/3\ Fe_3O_4 + 4H_2O,$$

such an estimate would be possible (see Turnock, 1960). This equilibrium will be dependent on the composition of the chlorite as well as the biotite.

The critical relationship, in all the above assemblages, is the coexistence of biotite, *magnetite*, and sanidine or muscovite. However, in many alteration sequences, the iron-rich minerals are sulfides rather than oxides, and consequently, the biotite mineral assemblages can provide useful constraints on intensive variables during the alteration.

In all these applications the maximum amount of information may be obtained only if the entire assemblage is considered, not merely the presence, absence, or composition of a single mineral. It is particularly valuable to determine the nature and composition of the opaque minerals ("ores") which are present. Also of great importance is the problem of contemporaneity of the several minerals.

Biotite Reaction Series

The reaction principle of Bowen (1922, 1928) applies to the biotites. The relations of biotite to a magmatic or metamorphic system will be quite sensitive to variations in temperature, pressure, or the activities of components such as O_2, H_2O, F, SiO_2. The types of reactions which can occur are highly varied but may be generalized to the form:

$$\text{biotite} + (O_2) + (SiO_2) \rightleftharpoons \text{K-feldspar (or feldspathoid)} + \text{Fe-Mg silicates (or oxides)} + H_2O.$$

The particular phases may be quartz, tridymite, sanidine, leucite, kalsilite, olivine, pyroxene, amphibole, magnetite, hematite, and/or a melt containing any or all of the critical components K_2O, Al_2O_3, SiO_2, MgO, Fe, O_2, H_2 and F.

The negative free energy of mixing for $KMg_3AlSi_3O_{10}(OH)_2$ and $KFe_3AlSi_3O_{10}(OH)_2$ indicates that biotites of intermediate compositions will coexist with more magnesian olivine, pyroxene or melt for magnesian bulk compositions and with more ferroan minerals for ferroan bulk compositions. Such relations are implied by Thompson (1957) in AFM diagrams for metamorphic assemblages, and by Larsen and Draisin (1948) for the igneous rocks of the southern California batholith. In other words, tie lines, biotite-ferromagnesian phase(s), are more concentrated near the middle of the phlogopite-annite series than they are near either of the two end members.

Heinrich (1946) and Nockolds (1947), in their analyses of biotite compositions in various rock types, showed some general trends which may be summarized by stating that the biotites from the more siliceous igneous rocks tend to be more iron-rich than biotites from the less siliceous rocks. There are two reasonable interpretations of these trends, one that the bulk compositions of these rock types are related and the biotites merely reflect that effect, or that the less siliceous rocks represent higher temperatures of crystallization and hence only Mg-rich biotites are stable at those magmatic conditions. The two interpretations are certainly not mutually exclusive.

The biotite data can be used to estimate the relative importance of intensive variables in establishing the distribution of iron and magnesium between various mafic phases. Heretofore, temperature and the nature of the coexisting phases were considered the most important variables. Figure 13 is an attempt to demonstrate, as shown by Muan and Osborn (1956), that f_{O_2} is as important as temperature, if the oxides are included as mafic phases. This figure also serves to summarize the biotite data. It is drawn for a constant (H_2+H_2O) pressure of 2070 bars and is a projection along the composition axis onto the f_{O_2}-T plane.

Figure 13 shows the projection of five sections made at constant bulk composition, represented by a specific biotite composition. These sections appear as the contours labelled 100, 70, 40, 30, and 0 and are the biotite-sanidine-magnetite contours of Fig. 4. They are drawn solid where they were located experimentally and are dashed where their position has been inferred. The contour labelled 0 represents the assemblage phlogopite+forsterite+leucite+kalsilite+gas. For annite bulk composition Eugster and Wones (1962) have shown that the sanidine +magnetite field cannot be in direct contact with the fayalite+leucite +kalsilite field, but must be separated from it by a narrow field representing the coexistence of fayalite+leucite+magnetite. The biotite +sanidine+magnetite field of Fig. 13 (field b), therefore, must also be separated from the biotite+olivine+leucite+kalsilite field (d) by a

narrow f_{O_2}-T area representing biotite+olivine+leucite+magnetite (field c, Fig. 13).

Since field c must exist for all biotite bulk compositions, the boundaries between fields b and c as well as c and d cannot cross the phlogopite contour, but must approach it gradually at some high f_{O_2}, at which neither the biotite nor the olivine will contain much iron. Thus a narrow strip of

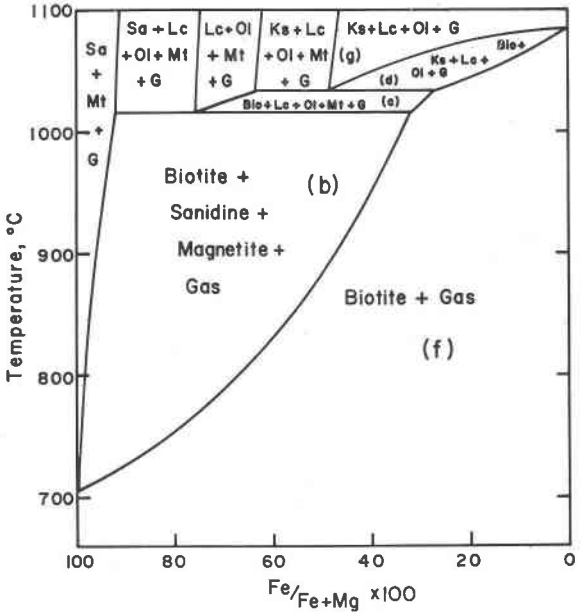

FIG. 14. T-X projection of $K(Fe,Mg)_3AlSi_3O_{10}(OH)_2+H_2+H_2O$ bulk composition, buffered by Fe_2SiO_4-Fe_3O_4-SiO_2, at a constant total pressure of 2070 bars. Only the boundary between fields (b) and (f) is experimentally determined.

the biotite-olivine-leucite-kalsilite field extends to high f_{O_2} values, but only for very magnesian bulk compositions. Where field c comes in contact with the f_{O_2}-T curve of the Fe_3O_4-Fe_2O_3 buffer, magnetite is replaced by hematite and the equivalent field c′ (biotite+olivine+leucite+hematite) extends into the hematite field.

It should be noted that a discontinuity must exist in the biotite contours where they cross boundaries between fields b, c (or c′) and d.

With the exception of field g, Fig. 13 only shows equilibria involving biotites. To clarify the high temperature relationships, Figure 14 has been constructed from Figure 13. It represents a T-X section along the f_{O_2}-T curve of the Fe_2SiO_4-Fe_3O_4-SiO_2 buffer (curve labelled 100 in Fig. 13). The biotite-sanidine-magnetite-gas boundary has been determined

experimentally up to a temperature of 900° C. (see Fig. 4). Above that temperature phase relations have been inferred from Fig. 13. In particular, the two isobaric invariant equilibria, biotite+sanidine+leucite +olivine+magnetite+gas and biotite+leucite+kalsilite+olivine +magnetite+gas, are shown which define the limits for field c. Fe/Fe +Mg ratios shown in Fig. 14 are those of coexisting biotites, olivines, and magnetites. At the highest temperatures and magnesium rich compositions a simple transition loop exists, enclosing the field of biotite+olivine+leucite+kalsilite+gas. At f_{O_2}-T values within the field of stability of wüstite, this transition loop would be continuous from the magnesium-free to the iron-free system.

In Fig. 13, equilibria existing at very low values of f_{O_2} have been partially omitted. Specifically, no field is shown for biotite+sanidine+iron. This assemblage would occupy a narrow strip within field e. In this f_{O_2}-T area a figure analogous to Figure 14 could be constructed, but with iron taking the place of magnetite. Because of the rapid decrease of f_{H_2O} at very low values of f_{O_2} for a P_{gas} of 2000 bars, all biotite contours must be crowded into the field representing biotite+sanidine+iron (within field e), as they pass towards lower temperatures and f_{O_2} values.

As mentioned above, Fig. 13 has also been constructed to elucidate relationships between several ferromagnesian phases. Therefore, the oxidation curves for fayalite 100, fayalite 10 forsterite 90, and fayalite 1 forsterite 99 have been projected onto the biotite-sanidine-magnetite field (in Fig. 13 these curves are labelled 100, ~10 and ~1, respectively. The 100 curve is, of course, the f_{O_2}-T curve of the Fe_2SiO_4-Fe_3O_4-SiO_2 buffer. The curves ~10 and ~1 were calculated assuming ideal cationic solid solutions in the olivines, an assumption justified by the theoretical analysis of Bradley (1962). The Fa_{10} and Fa_1 contours indicate the fayalite contents of olivines from olivine-pyroxene-magnetite assemblages and represent the highest Fe_2SiO_4 content possible for the given f_{O_2}-T values. The olivine and biotite contours intersect at steep angles, because the olivine contours represent redox reactions while the biotite contours represent hydrogenation-dehydrogenation reactions.

If we consider biotite-olivine bulk compositions, that is, the assemblages biotite-olivine-sanidine-magnetite-(quartz)-(pyroxene), we can predict accurately the effects of both f_{O_2} and T on the magnesium-iron distribution between biotite and olivine. At constant temperature, for example, an increase in oxygen pressure will not only result in a decrease in the iron content of both the stable biotite and the stable olivine. Pyroxenes should behave very similarly to olivines, since pyroxene contours (Fig. 12) also represent simple redox reactions. Consequently, if the f_{O_2}-T conditions are appropriate, the iron-magnesium distribution of

biotite-olivine or biotite-pyroxene pairs may favor either iron-rich biotite coexisting with magnesian olivine and pyroxene (Pecora, 1941; Ramberg, 1952) or magnesium-rich biotite coexisting with iron-rich pyroxene (Larsen and Draisin, 1948).

Changes in H_2+H_2O pressure basically have little effect on the spatial relations of the equilibria shown in Fig. 13. Increasing pressure merely shifts the biotite contours towards higher temperatures, while the olivine contours remain practically unaffected.

Figure 13 represents, of course, unusual bulk compositions. Amphiboles and pyroxenes are much more commonly associated with biotites than are olivines. But for such assemblages no data are available and no valid extrapolations are possible at this time.

We may now attempt to discuss biotites in equilibrium with a melt. The biotite contours of Fig. 13 can probably be safely extended to include biotite+sanidine+magnetite+melt. These four phases act as f_{o_2} buffers and changes in the Mg/Fe ratio of the melt would simply be reflected in the amounts of biotite and magnetite coexisting with the melt. Osborn (1962) has emphasized the importance of f_{o_2} on the course of crystallization of magmas and on the end products. In a similar way we may consider two contrasting trends of crystallization (Fig. 13).

Trend I represents a magma, which, during crystallization and cooling, becomes saturated in H_2O, reacts with that component, and loses hydrogen to the environment. In such a situation f_{O_2} remains constant or increases slightly with little change or a decrease in the Fe/Fe+Mg ratio of the biotites crystallizing from the melt. The final crystallization products will be magnesium-rich biotite and considerable quantities of magnetite. Grout (1923) described such phenomena in the granite of St. Louis County, Minnesota. Potapiev (1964) has described such phenomena in the Kolyvanian massif, and one of us (D.R.W.) on field trips with P. C. Bateman has observed such sequences in the late stages of crystallization in the plutons of the Sierra Nevada batholith (Bateman *et al.*, 1963).

Trend II, represents a magma which, because of the low H_2O content, is "buffered" by the anhydrous mineral assemblages. The final result would be the crystallization of iron-rich biotite and other ferromagnesian silicates and very little magnetite. Larsen and Draisin (1948) indicate that this may be the case for portions of the southern California batholith, and the data of Heinrich (1946) and Nockolds (1947) imply this situation may be the more general case.

It would seem that the relations of the several ferromagnesian minerals in a crystallization sequence might indicate a probable f_{o_2}-T path of the crystallizing magma, and this, in turn, might give some indication

of H_2O saturation of undersaturation. The problem of H_2 solubility and diffusion in silicate melts also must be considered.

Biotites as Indicators of Intensive Variables

The biotite stability has been shown to be bounded by a trivariant equilibrium such that in the assemblage biotite-K-feldspar-magnetite three of the four variables, mol fraction of $KFe_3AlSi_3O_{10}(OH)_2$, oxygen fugacity, H_2O fugacity, and temperature, must be defined before the fourth can be determined. Additional complications involve the mol fractions of $KAlSi_3O_8$ and Fe_3O_4 in the feldspar and spinel phases, as well as the structural state of the feldspar. For such cases expression (6″) must be used. The problem of estimates of $a_{KAlSi_3O_8}$ and $a_{FeO_{34}}$ is best solved by using the data or Orville (1963) for $KAlSi_3O_8$ activities, and those of Lindsley (1963) and Turnock and Eugster (1962) for the Fe_3O_4 activities.

Once that assemblage has been established, however, it is relatively straightforward to determine f_{H_2O}, given f_{O_2}, and T. The remaining problems thus consist of getting estimates of two intensive variables. Lindsley's (1963) data on the system Fe-Ti-O provide means of estimating f_{O_2}-T conditions from the composition of the coexisting iron and titanium oxides.

Biotite analyses may also provide rough estimates of f_{O_2}-T conditions at constant f_{H_2O}. From Fig. 1 it can be seen that $Fe^{3+}/Fe^{2+}+Fe^{3+}$ is about 0.25 for Fe_3O_4-Fe_2O_3 buffer conditions; 0.10 for Ni-NiO; 0.05 for Fe_2SiO_4-Fe_3O_4-SiO_2; and <0.02 for $Fe_{1-x}O$-Fe_3O_4.

For temperature estimates there are such possibilities as the feldspar solvus (Yoder, *et al.*, 1957; Wyart and Sabatier, 1962; and Orville, 1963), the calcite-dolomite solvus (Goldsmith, 1959) muscovite-paragonite solvus (Eugster, 1956), and isotope fractionation (Epstein, 1959).

The fugacity of H_2O is probably one of the more interesting variables to attempt to define, as f_{H_2O} influences melting points (Tuttle and Bowen, 1958), viscosities (Shaw, 1963b; Friedman *et al.*, 1963; Burnham, 1964) eruptive phenomena (Boyd, 1961; McBirney, 1963) and metamorphic grade (Fyfe, *et al.* 1958). If f_{O_2} and T can be estimated, the biotites should serve as indicators of f_{H_2O}. Even in the absence of K-feldspar and magnetite the mol fraction of $KFe_3AlSi_3O_{10}(OH)_2$ in biotite permits minimum estimates of f_{H_2O} to be made.

Of the many biotite-K-feldspar-magnetite assemblages described in the literature, the two selected here demonstrate different applications of the biotite data. The study of Larsen *et al.* (1937) on phenocrysts in volcanic rocks demonstrates the usefulness of the stability data with even a limited amount of information on the composition of the biotite. The combined data of Engel and Engel (1960) and Buddington (1963)

provide an example where a more rigorous application can be made because of an abundance of mineralogical information.

Volcanic Rocks. The data of Larsen *et al.* (1937) on the biotites found in the quartz-latites of the San Juan Mountains, Colorado, when combined with the Tuttle and Bowen (1958) minimum melting curve, permit a very rough estimate of the f_{H_2O}-T conditions of the magma chamber at the time of eruption. The biotites in question have been badly oxidized

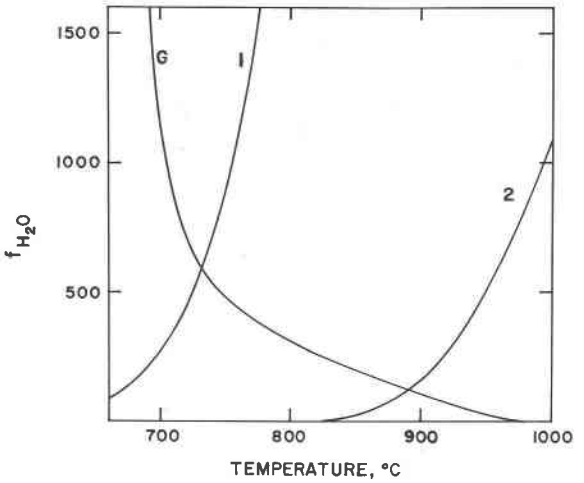

FIG. 15. Plot of f_{H_2O} versus T for G, "granite minimum melting" as determined by Tuttle and Bowen (1958). Curve 1 represents the stability a biotite of 0.15 mol fraction $KFe_3AlSi_3O_{10}(OH)_2$ coexisting with magnetite and hematite. Curve 2 represents the stability of a biotite of 0.25 mol fraction $KFe_3AlSi_3O_{10}(OH)_2$ coexisting with quartz, magnetite, and fayalite.

during the eruptive history so that it is difficult to obtain an estimate of f_{O_2}. In the example of the Piedra Rhyolite, the mol fraction of $KFe_3AlSi_3O_{10}(OH)_2$ end member is about 0.28 ± 0.03. Assuming that Fe_3O_4-Fe_2O_3 and Fe_2SiO_4-SiO_2-Fe_3O_4 are the limiting f_{O_2}-T boundaries, the stability curves for a biotite of this composition may be calculated from equation (6′) and are shown intersecting Tuttle and Bowen's (1958) minimum melting curve at either 730° C., 600 bars f_{H_2O} or 875° C., 125 bars f_{H_2O} in Fig.15. Tuttle and Bowen's data were recast in fugacities rather than pressures. The need for most precise information is obvious, and careful examination of the oxide minerals could permit a better estimate.

In the above example the mol fraction of $KFe_3AlSi_3O_{10}(OH)_2$ was assumed to be 0.15 in the first case and 0.25 in the second. These values re-

fer to Fig. 1 which shows estimates of $KFe_3AlSi_3O_{10}(OH)_2$ concentrations in biotites buffered by Fe_2SiO_4-Fe_3O_4-SiO_2 and Fe_3O_4-Fe_2O_3. The major assumption in this treatment is that components other than Mg^{2+} have the same effect on the stability of the annite end member. Minor assumptions are that the activities of $KAlSi_3O_8$ and Fe_3O_4 are 1, and that the melting curve of the Piedra Rhyolite is comparable to the "granite minimum" melting curve.

The presence of a biotite phenocryst of known composition permits a minimum H_2O fugacity to be estimated for a given temperature, whereas the presence of magnetite or pyroxene (Carmichael, 1960) to the exclusion of biotite permits a maximum estimate for the H_2O fugacity.

Metamorphic Rocks. The complete data of Engel and Engel (1958, 1960) on biotite-sanidine-magnetite assemblages, when combined with the approximate magnetite compositions given by them, permit fairly good estimates of f_{H_2O} during regional metamorphism of the gneisses of the Northwest Adirondacks. In this case the f_{O_2} estimates are much better, as both Lindsley's (1963) data on the system Fe-Ti-O and the Fe^{3+} content of the biotite permit estimates to be made of f_{O_2}-T conditions.

Engel and Engel (1958, 1960) have estimated the temperatures of two assemblages in gneissic rocks to be 500° and 600°, respectively. For the 500° C. assemblage (Emeryville), the Fe^{2+} content of the biotite octahedral layer is about .38, the Fe^{3+} content is about 0.04. The feldspar is about Or_{81} and the ulvöspinel content of the magnetite may be estimated at 0.04. For the 600° C. (Colton) assemblage, the biotite has an Fe^{2+} content of 0.30, and Fe^{3+}, 0.03. The feldspar is Or_{79} and the ulvöspinel content of the magnetite is about 0.08.

For the 500° assemblage the biotite data imply an f_{O_2} of 10^{-23} to 10^{-25}. The ulvöspinel content of the magnetite implies a similar value. The coexistence of quartz and magnetite place a minimum limit of f_{O_2} at 10^{-25}. The data for the 600° assemblage imply values of 10^{-18} to 10^{-19}, however 10^{-21} is the minimal limit.

The remaining assumptions are concerned with the deviation of the activities of $KAlSi_3O_8$ and Fe_3O_4. Although Lindsley's (1963) data demonstrate the nonideal behaviors of Fe_3O_4-Fe_2TiO_4 solid solutions, for these calculations the assumption of ideality was used, $a_{Fe_3O_4} = x_{Fe_3O_4}$. Orville's (1963) data for alkali feldspars coexisting with aqueous chloride solutions have been used to estimate the activities of $KAlSi_3O_8$ in alkali feldspar. For the 500° assemblage, a value of 0.81 was assigned to $a_{KAlSi_3O_8}$, and for 600°, 0.79.

Applying these values to equation (6″) one obtains the expression $\log f_{H_2O} = \log f_{O_2}^{\frac{1}{2}} + 11.09$ at 500° C. and $\log f_{H_2O} = \log f_{O_2}^{\frac{1}{2}} + 10.13$ at 600° C. If

f_{O_2} at 500° C. was 10^{-24} bars then f_{H_2O} must be about 0.1 bar; at 600° C. f_{H_2O} must vary between 1–10 bars.

The gneisses in the Adirondacks are interlayered with graphitic marbles and amphibolites. The amphibolites have clinopyroxene-pyroxene-hornblende assemblages (Engel and Engel, 1962). Extrapolating the data of Boyd (1959) on the tremolite$\rightleftharpoons$diopside+enstatite+quartz+H_2O reaction to 500° and 600° C., the equilibrium H_2O pressures are about 0.1 and 1 bar.

The graphite-CO_2 reaction has been recently studied by French (1964) using the data of Wagman *et al.* (1945). For graphite one may obtain, at 500° C., the expression $\log f_{CO_2} = \log f_{O_2} + 26.64$ and at 600° C., $\log f_{CO_2} = \log f_{O_2} + 23.60$. The values of $\log f_{CO_2}$ obtained for the Adirondack assemblages are 2.60 at 500° C. and 4.00 at 600° C. This disparity may be explained in terms of disequilibrium, a lack of graphite in the 600° C. assemblage, or the actual gradient in the fugacity of CO_2 from 435 to 10,000 bars. The high ratios of CO_2 to H_2O are consistent with the mineral assemblages of the marbles and the interbedded gneisses, so that the gradient may well exist and be due to dehydration and decarbonation reactions leading to the high temperature assemblage.

If the biotites are not in equilibrium with the magnetites, then the H_2O fugacities are minimal values. However, the decrease in the quantity of biotite, the variations in magnetite composition, and the presence of graphite in the marbles all combine to give a uniform model.

A further implication of the data is that the existence of biotite-K-feldspar-magnetite assemblages in rocks of low metamorphic grade ($<500°$ C.) implies very low values for water pressure, and perhaps many models in which water pressure is considered equal to load pressure need revision.

Detection of Gradients. The fact that the composition of biotite coexisting with sanidine and magnetite is dependent on f_{H_2O}, f_{O_2} and T implies that gradients in any of these three intensive variables should be reflected in changes in the composition of biotite. Peikert (1963) applied this argument with some success to rocks of the Canadian Shield in northeastern Alberta. He found that biotite compositions were closely related to specific rock types. He assumed that rocks of such close proximity would be isothermal, so that variations in f_{O_2} or f_{H_2O} were responsible for the deviations in the composition of the biotites. If the gneisses are formed by the alteration of metasedimentary rocks, the model of cation exchange from an ubiquitous vapor phase in such a system is difficult to reconcile with the persistence of steep gradients in f_{O_2} observed in many localities (Chinner, 1960; Eugster, 1959). Pitcher and Sinha (1957) have observed

mineralogic changes easily explained by gradients in the f_{O_2} of contact aureoles around granite intrusives.

The changes in the compositions of biotites in wall rock alteration processes (Anderson *et al.*, 1955) very clearly show gradients in the activities of oxygen and sulfur which also match the activity gradients proposed for H^+ and K^+ in such phenomena. The stability of biotite in such phenomena is also a function of other variables such as the hydrogen ion and potassium ion concentrations.

Biotites in Geochronology

The high K and Rb contents of biotites have made them valuable for studies in geochronology, using the K-Ar and Rb-Sr methods for dating the time of crystallization of the biotite. As this study has shown, the biotite-K-feldspar-magnetite assemblage represents a trivariant equilibrium in which changes in P, T, f_{H_2O}, or f_{O_2} will necessitate a change in the composition of biotite through recrystallization in order to reestablish equilibrium.

The classic study of Tilton *et al.* (1958) on the Baltimore Gneiss demonstrated that the ages of the biotites are Paleozoic, but the ages of the zircons and feldspars are Precambrian. As all the biotites examined are in K-feldspar and magnetite bearing assemblages (C. A. Hopson, 1964, and pers. comm.), recrystallization of the biotites during metamorphism seems entirely reasonable. Jaeger *et al.* (1961) have also demonstrated variations in biotite ages in which the biotites are partially recrystallized. Recently, however, Tilton and Hart (1963) have shown that diffusion of argon and strontium out of biotite crystals during metamorphism will reduce biotite ages without recrystallization.

It is readily apparent that biotite ages are particularly subject to metamorphic changes. Careful petrographic studies to ascertain either the homogeneity of the biotites being analysed or the existence of the trivariant assemblages discussed certainly should add a great deal to the interpretation of biotite ages. Biotites occurring in K-feldspar, muscovite, or magnetite free assemblages (marble, quartz-plagioclase-biotite gneisses) should have less tendency to recrystallize, and *might* be expected to yield older ages.

Acknowledgments

This study was initiated at the Geophysical Laboratory, Carnegie Institution Washington, while D. R. Wones held a Vannevar Bush Fellowship and H. P. Eugster was a staff member. D. R. Wones would like to express his gratitude to the Geology Department of the Massachusetts

Institute of Technology and to the Geophysical Laboratory for making this opportunity available, as well as to Profs. H. W. Fairbairn and G. J. F. MacDonald of M.I.T. and to Prof. J. B. Thompson, Jr. of Harvard University for much help and stimulation at the beginning of this study.

We are much indebted to our colleagues at the Geophysical Laboratory, the U. S. Geological Survey and The Johns Hopkins University for encouragement and many helpful discussions. The manuscript was critically reviewed by J. J. Hemley, H. R. Shaw and Priestly Toulmin, III, and their comments led to a considerable improvement of the manuscript.

References

Anderson, C. A., E. A. Scholz and J. D. Strobell, Jr. (1955) Geology and ore deposits of the Bagdad area, Yavapai County, Arizona. *U. S. Geol. Survey Prof. Paper* **278.**

Bartholmé, Paul (1962) Iron-magnesium ratio in associated pyroxenes and olivines. In *Geol. Soc. Am. Petrologic studies: a Volume in Honor of A. F. Buddington.* 1–20.

Bateman, P. C., L. D. Clark, N. K. Huber, J. G. Moore and C. D. Rinehart (1963) The Sierra Nevada batholith: A synthesis of recent work across the central part. *U. S. Geol. Survey Prof. Paper 414-D.*

Blumenthal, R. N. and D. H. Whitmore (1961) Electrochemical measurements of elevated-temperature thermodynamic properties of certain iron and manganese oxide mixtures. *Jour. Am. Ceram. Soc.* **44,** 508–512.

Bowen, N. L. (1922) The reaction principle in petrogenesis. *Jour. Geol.* **30,** 177–198.

——— (1928) *The Evolution of the Igneous Rocks.* Univ. Press, Princeton, N.J.

——— and J. F. Schairer (1935) The system, MgO-FeO-SiO_2. *Am. Jour. Sci.* Ser. 5, **29,** 151–217.

Boyd, F. R. (1959) Hydrothermal investigations of amphiboles *in* P. H. Abelson, ed., *Researches in Geochemistry.* John Wiley & Sons, N. Y., 377–396.

——— (1961) Welded tuffs and flows in the rhyolite plateau of Yellowstone Park, Wyoming. *Geol. Soc. Am. Bull.* **72,** 387–426.

Bradley, R. S. (1962) Thermodynamic calculations on phase equilibria involving fused salts. Part II, Solid solutions and application to the olivines. *Am. J. Sci.* **260,** 550–554.

Buddington, A. F. (1963) Isograds and the role of H_2O in metamorphic facies of orthogneisses of the northwest Adirondack Area, New York: *Geol. Soc. Am. Bull.* **74,** 1155–1182.

Burnham, C. W. (1964) Viscosity of a water-rich pegmatite melt at high pressures (abs.). *Geol. Soc. Am. Spec. Paper* **76,** 26.

Carmichael, I. S. E. (1960) The pyroxenes and olivines from some Tertiary acid glasses. *Jour. Petrology,* **1,** 309–336.

Chinner, G. A. (1960) Pelitic gneisses with varying ferrous-ferric ratios from Glen Clova, Angus, Scotland. *Jour. Petrology,* **1,** 178–217.

Deer, W. A., R. A. Howie and J. Zussman (1962) *Rock Forming Minerals:* v. 5, *Non-silicates.* John Wiley & Sons, N.Y.

Donnay, G. and J. D. H. Donnay (1952) The symmetry change in the high temperature alkali feldspar series. *Am. Jour. Sci., Bowen Vol.* 115–132.

Donnay, J. D. H. and W. Nowacki (1954) Crystal Data. *Geol. Soc. Am. Mem.* **60.**

ENGEL, A. E. J. AND C. ENGEL (1958, 1960) Progressive metamorphism and granitization of the major paragneiss, northwest Adirondack Mountains, New York: Pt. 1. Total rock; Pt. 2, Mineralogy. *Geol. Soc. Am. Bull.* **69,** 1369–1413, 1958; **71,** 1–58, 1960.

——— (1962) Progressive metamorphism of amphibolite, northwest Adirondack Mountains, New York. In *Geol. Soc. Am., Petrologic studies: a Volume in Honor of A. F. Buddington.* 37–82.

EPSTEIN, S. (1959) The variations of the O^{18}/O^{16} ratio in nature and some geologic implications. In P. H. Abelson, ed., *Researches in Geochemistry.* John Wiley & Sons., N. Y., 217–240.

EUGSTER, H. P. (1956) Muscovite-paragonite join and its use as a geologic thermometer. *Geol. Soc. Am. Bull.*, **67,** 1693.

——— (1957) Heterogeneous reactions involving oxidation and reduction at high pressures and temperatures. *Jour. Chem. Physics.* **26,** p. 1160.

——— (1959) Reduction and oxidation in metamorphism. In P. H. Abelson, ed., *Researches in Geochemistry.* John Wiley & Sons, N. Y. 397–426.

——— AND D. R. WONES (1962) Stability relations of the ferruginous biotite, annite. *Jour. Petrology,* **3,** 82–125.

——— AND H. S. YODER (1956) Paragonite. *Ann Rept. Director Geophys. Lab.*, 1955–1956, *Carnegie Inst. Wash. Yearbook* **55,** 124–126.

FOSTER, M. D. (1960) Interpretation of the composition of trioctahedral micas. *U. S. Geol. Survey Prof. Paper* **354-B,** 11–49.

FRENCH, B. M. (1964) Stability of siderite and the progressive metamorphism of iron formation. Ph.D. Thesis, The Johns Hopkins University, Baltimore, Maryland.

FRIEDMAN, I., W. LONG AND R. L. SMITH (1963) Viscosity and water content of rhyolite glass. *Jour. Geophys. Res.* **68,** 6523–6535.

FYFE, W. S., F. W. TURNER AND J. VERHOOGEN (1958) Metamorphic reactions and metamorphic facies. *Geol. Soc. Am. Mem.* **73.**

GHOSE, SUBRATA (1962) The nature of Mg^{2+}-Fe^{2+} distribution in some ferromagnesian silicate minerals. *Am. Mineral.* **47,** 388–394.

GOWER, J. A. (1957) *X*-ray measurement of the iron magnesium ratio in biotites. *Am. Jour. Sci.* **225,** 142–156.

GOLDSMITH, J. R. (1959) Some aspects of the geochemistry of carbonates. In P. H. Abelson, ed., *Researches in Geochemistry.* John Wiley & Sons, N. Y. 336–358.

GROUT, F. F. (1923) Magnetite pegmatites of Northern Minnesota. *Econ. Geol.* **18,** 253–269.

GUGGENHEIM, E. A. (1952) *Mixtures.* Oxford Univ. Press.

HEINRICH, E. WM. (1946) Studies in the mica group: The biotite-phlogopite series. *Am. Jour. Sci.* **244,** 836–853.

HOLSER, W. T. (1954) Fugacity of water at high temperatures and pressures. *Jour. Phys. Chem.* **58,** 316–317.

HOPSON, C. A. (1964) The crystalline rocks of Howard and Montgomery Counties. In Cloos, E. and others, The Geology of Howard and Montgomery Counties. *Maryland Geol. Survey,* 27–215.

JAEGER, E., E. KEMPTER, E. NIGGLI AND H. M. WÜTHRICH (1961) Biotit-Varietäten und Stilpnomelan im Alpin Metamorph überprägten Mittagfluh-Granit (Aarmassiv). *Schweiz. Mineral. Petro. Mitt.* **41,** 117–126.

KRETZ, RALPH (1964) Analysis of equilibrium in garnet-biotite-sillimanite gneisses from Quebec. *Jour. Petrology,* **5,** 1–20.

LARSEN, E. S., JR., J. IRVING, F. A. GONYER AND E. S. LARSEN, 3rd. (1937) Petrologic results of a study of the minerals from the Tertiary volcanic rocks of the San Juan region, Colorado. *Am. Mineral.* **22,** 889–905.

——— AND W. M. DRAISIN (1948) Composition of the minerals in the rocks of the southern California batholith. *Inter. Geol. Cong., Great Britain, Sess.* XVIII, 66–79.

LINDSLEY, D. H. (1963) Fe-Ti oxides in rocks as thermometers and oxygen barometers. *Ann. Rept. Director Geophys. Lab.*, 1962–1963, *Carnegie Inst. Washington:* Year Book **62,** 60–66.

LUTH, W. C. (1964) Invariant and univariant equilibria in the system $KAlSiO_4$-Mg_2SiO_4-SiO_2-H_2O (abs.). *Trans. Am. Geophys. Union,* **45,** 125–126.

MCBIRNEY, A. R. (1963) Factors governing the nature of submarine volcanism. *Bull. Volcano.* **26,** 455–469.

MUAN, A. (1963) Silver-palladium alloys as crucible material in studies of low-melting iron silicates: *Am. Ceram. Soc. Bull.* **46,** 344–347.

——— AND E. F. OSBORN (1956) Phase equilibria at liquidus temperatures in the system MgO-FeO-Fe_2O_3-SiO_2. *Am. Ceram. Soc. Jour.* **39,** 121–140.

MUELLER, R. F. (1960) Compositional characteristics and equilibrium relations in mineral assemblages of a metamorphosed iron formation. *Am. Jour. Sci.* **258,** 449–497.

NOCKOLDS, S. R. (1947) The relation between chemical composition and paragenesis in the biotite micas of igneous rocks. *Am. Jour. Sci.* **245,** 401–420.

NORTON, F. J. (1955) Dissociation pressures of iron and copper oxides. *General Electric Res. Lab. Rept.* **55-RL-1248.**

ORVILLE, P. M. (1963) Alkali ion exchange between vapor and feldspar phases. *Am. Jour. Sci.* **261,** 201–237.

OSBORN, E. F. (1962) Reaction series for subalkaline igneous rocks based on different oxygen pressure conditions. *Am. Mineral.* **47,** 211–226.

PECORA, W. T. (1941) Structure and petrology of the Boxelder laccolith, Bearpaw Mountains, Montana. *Geol. Soc. Am. Bull.* **52,** 817–854.

PEIKERT, E. W. (1963) Biotite variation as a guide to petrogenesis of granitic rocks in the Pre-Cambrian of northeastern Alberta. *Jour. Petrology,* **4,** 432–459.

PITCHER, W. S. AND R. C. SINHA (1957) The petrochemistry of the Ardara aureole. *Quart. Jour. Geol. Soc. London,* **113,** 393–408 [1958]

POTAPIEV, V. V. (1964) On the drop in the refraction indices of biotites in granites of late phases of the Kolyvanian massif (Atlai). *Doklady Akad. Nauk SSSR,* **155,** 583–585.

RAMBERG, HANS (1952) Chemical bonds and distribution of cations in silicates. *Jour. Geol.* **60,** 331–355.

RICCI, J. E. (1951) *The Phase Rule and Heterogeneous Equilibrium.* D. Van Nostrand Co. Inc., New York.

ROBIE, R. A. (1962) Thermodynamic properties of minerals. *U. S. Geol. Survey Rept.* **TEI-816,** open-file report.

——— AND P. M. BETHKE (1963) Molar volumes and densities of minerals. *U. S. Geol. Survey Rept.* **TEI-822,** open-file report.

SCHAIRER, J. F. (1954) The system K_2O-MgO-Al_2O_3-SiO_2. *Am. Ceram. Soc. Jour.,* **37,** 501–533.

SEGNIT, R. E. AND G. C. KENNEDY (1962) Reactions and melting relations in the system muscovite-quartz at high pressures. *Am. Jour. Sci.* **259,** 280–287.

SHAW, H. R. (1963a) Hydrogen-water vapor mixtures: Control of hydrothermal atmospheres by hydrogen osmosis. *Science,* **139,** 1220–1222.

——— (1963b) Obsidian-H_2O viscosities at 1000 and 2000 bars in the temperature range 700° to 900° C. *Jour. Geophys. Res.* **68,** 6337–6344.

——— (1963c) The four-phase curve sanidine-quartz-liquid-gas between 500 and 4000 bars. *Am. Mineral.* **48,** 883–896.

——— AND D. R. WONES (1964) Fugacity coefficients for hydrogen gas between 0° and 1000° C., for pressures to 3000 atm. *Am. Jour. Sci.*, **262,** 918–929.

SMITH, J. V. AND H. S. YODER, JR. (1956) Experimental and theoretical studies of the mica polymorphs. *Mineral. Mag.* **31,** 209–235.

THOMPSON, J. B. (1957) The graphical analysis of mineral assemblages in pelitic schists. *Am. Mineral.* **42,** 842–858.

TILLEY, C. E. (1957) Problems of alkali rock genesis. *Quart. Jour. Geol. Soc. London,* **113,** 323–360.

TILTON, G. R. AND S. R. HART (1963) Geochronology. *Science,* **140,** 357–366.

——— G. W. WETHERILL, G. L. DAVIS AND C. A. HOPSON (1958) Ages of minerals from the Baltimore gneiss near Baltimore, Maryland. *Geol. Soc. Am. Bull.* **69,** 1469–1474.

TURNOCK, A. C. (1960) The stability of iron chlorites. *Ann. Rept. Director Geophys. Lab.* 1959–1960, *Carnegie Inst. Washington Year Book* **59,** 98–103.

——— AND H. P. EUGSTER (1962) Fe-Al oxides: Phase relationships below 1000° C. *Jour. Petrology,* **3,** 533–565.

TUTTLE, O. F. (1952) Optical studies on alkali feldspars. *Am. Jour. Sci., Bowen Vol.* 553–567.

——— AND N. L. BOWEN (1958) Origin of granite in the light of experimental studies in the system $NaAlSi_3O_8$-$KAlSi_3O_8$-SiO_2-H_2O. *Geol. Soc. Am. Mem.* **74.**

VELDE, B. (1964) Upper stability of muscovite. *Ann. Rept. Director Geophys. Lab.,* 1963–1964, *Carnegie Inst. Washington, Year Book* **63,** 141–142.

WAGMAN, D. D., J. E. KILPATRICK, W. J. TAYLOR, K. S. PITZER AND F. E. ROSSINI (1945) Heats, free energies, and equilibrium constants of some reactions involving O_2, H_2, H_2O, C, CO, CO_2 and CH_4. *Jour. Res. Natl. Bur. Stand.* **34,** 143–161.

WONES, D. R. (1963a) Phase equilibria of "ferriannite," $KFe_3^{+2}Fe^{+3}Si_3O_{10}(OH)_2$. *Am. Jour. Sci.* **261,** 581–596.

——— (1963b) Physical properties of synthetic biotites on the join phlogopite-annite. *Am. Mineral.* **48,** 1300–1321.

——— AND D. E. APPLEMAN (1961) *X*-ray crystallography and optical properties of synthetic monoclinic $KFeSi_3O_8$, iron-sanidine. *U. S. Geol. Survey Prof. Paper* **424-C,** C309-C310.

WYART, J. AND G. SABATIER (1962) Sur le problème de l'équilibre des feldspars alcalins et des plagioclases. *Acad. Sci.* (Paris) *Compt. Rend.* **255,** 1551–1554.

YODER, H. S., JR. AND H. P. EUGSTER (1954) Phlogopite synthesis and stability range: *Geochim. Cosmochim. Acta.* **6,** 157–185.

——— D. B. STEWART AND J. R. SMITH (1957) Ternary feldspars. *Ann. Rept. Director Geophys. Lab.,* 1956–1957, *Carnegie Inst. Washington Yearbook* **56,** 206–214.

Manuscript received, January 29, 1965; accepted for publication, May 4, 1965.